

UNIVERSITY OF MALTA

Institute for Sustainable Energy

M.Sc. Dissertation

Determining the Typical Meteorological Year for the Maltese
Islands

By

Daniel Spiteri

A dissertation submitted in partial fulfilment of the requirements of the award of
Master of Science in Sustainable Energy

May 2022



L-Università
ta' Malta

University of Malta Library – Electronic Thesis & Dissertations (ETD) Repository

The copyright of this thesis/dissertation belongs to the author. The author's rights in respect of this work are as defined by the Copyright Act (Chapter 415) of the Laws of Malta or as modified by any successive legislation.

Users may access this full-text thesis/dissertation and can make use of the information contained in accordance with the Copyright Act provided that the author must be properly acknowledged. Further distribution or reproduction in any format is prohibited without the prior permission of the copyright holder.

Copyright Notice:

1) Copyright in text of this dissertation rests with the Author. Copies (by any process) either in full, or of extracts may be made only in accordance with regulations held by the Library of the University of Malta. Details may be obtained from the Librarian. This page must form part of any such copies made. Further copies (by any process) made in accordance with such instructions may not be made without the permission (in writing) of the Author.

2) Ownership of the right over any original intellectual property which may be contained in 4 or derived from this dissertation is vested in the University of Malta and may not be made available for use by third parties without the written permission of the University, which will prescribe the terms and conditions of any such agreement.”

Abstract

Typical meteorological year (TMY) data files are becoming increasingly in demand especially to serve as input to building energy modelling software, which requires representative hourly dataset of one year. The dataset should contain all relevant meteorological parameters, such as dry bulb temperature, dew point temperature, wind speed and wind direction, global and diffuse solar radiation, relative humidity, and atmospheric pressure. Several methods by which such an hourly TMY can be derived from a long-term dataset exist. These methods apply various statistical tools and selection criteria to select the most representative months from the available set of weather data files. The selected months are then concatenated to form what is known as the TMY.

The main aim of this dissertation was to build the TMY for the Maltese Islands for its implementation in building energy performance software. Different methodologies were applied to a 13-year dataset of meteorological measurements from an onshore site in the Maltese Islands and five TMYs were generated. The TMYs were statistically compared to the long-term weather behaviour and the most representative TMY was determined.

From the analyses carried out it was found that overall, the most representative TMY was the one yielded by a variant of the Festa-Ratto method developed by Festa and Ratto. The other methods produced TMYs with varying degrees of representation.

Acknowledgements

I would like to express my appreciation towards a number of people who played an important role during this dissertation. I would first like to thank Dr. Ing. Charles Yousif for providing the opportunity of developing a typical meteorological year for the Maltese Islands and for continuously guiding me during the course of this dissertation. I would also like to thank Dr. Ing. Robert N Farrugia whose contributions were important. The entire staff within the Institute for Sustainable Energy merits appreciation for their insightful teachings during the course of studies. Lastly, heartfelt thanks go to my family and friends for their support during these past years.

Table of Contents

1	Introduction.....	1
1.1	Climate change: Evidence and Effects.....	1
1.2	Climate change mitigation.....	9
1.3	Energy performance of buildings.....	12
1.4	Objectives and structure	14
2	Literature Review	17
2.1	Introduction	17
2.2	The Solar Cycle.....	17
2.3	Typical Meteorological Year (TMY) – Definition and Methods	21
2.3.1	Statistical tools.....	23
2.3.2	TMY Methods.....	26
2.4	Characteristics of the Maltese Climate	33
3	Methodology.....	36
3.1	Weather Data Quality Control	36
3.2	TMY Methods.....	38
3.3	Selecting the most representative TMY	40
4	Results and Analyses.....	41
4.1	Results.....	41
4.1.1	Quality Control.....	41
4.1.2	Typical Meteorological Months	43
4.2	Analysis.....	44
4.2.1	Descriptive Statistics.....	44
4.2.2	Frequency Analysis.....	54
4.2.3	Wind direction distributions – the wind roses	59
4.2.4	CDF Analysis and selection of TMY	62

5	Conclusions and Recommendations.....	69
5.1	Conclusion.....	69
5.2	Further Work.....	71
6	References.....	73

List of Figures

Figure 1: The layers of Earth’s atmosphere [3]	2
Figure 2: Global annual total CO ₂ emission by continent over the period 1750 – 2019 [6].	3
Figure 3: Global average surface temperature anomaly (1880 – 2020) [15].....	5
Figure 4: Cumulative ice mass loss from the Greenland and Antarctic ice sheets [22].....	8
Figure 5: The Climate Action Tracker thermometer showing projected temperature increases by 2100 [21]	11
Figure 6: 2018 global GHG Emissions from CAIT data [23].....	12
Figure 7: A coronal loop emerging from a pair of sunspots [29].....	18
Figure 8: Solar irradiance and sunspot number in the era of satellite data [31].....	20
Figure 9: A montage of images of the sun spanning between 1991 and 2001 obtained from the Yohkoh solar observatory spacecraft [31]	20
Figure 10: Monthly mean dry bulb temperatures (°C) of TMY methods and long-term data	50
Figure 11: Monthly mean wind speed (m s ⁻¹) of TMY methods and long-term data.....	50
Figure 12: Monthly sum of global solar radiation (KW h m ⁻²) of TMY methods and long-term data	51
Figure 13: Daily mean dry bulb temperatures (°C) of TMY methods and long-term average data	52
Figure 14: Daily mean wind speed (m s ⁻¹) of TMY methods and long-term average data .	52
Figure 15: Daily sum of global solar radiation (W h m ⁻²) of TMY methods and long-term average data	53
Figure 16: Daily mean dry bulb temperature (°C) histogram for TMYs and long-term data	56
Figure 17: Daily mean wind speed (m s ⁻¹) histogram for TMYs and long-term data	56
Figure 18: Daily sum of global solar radiation (W h m ⁻²) histogram for TMYs and long-term data	57
Figure 19: Wind rose for 2007-2019 hourly measurements.....	60
Figure 20: Wind rose for TMY _{S1} hourly measurements.....	60
Figure 21: Wind rose for TMY _{S2} hourly measurements.....	60
Figure 22: Wind rose for TMY _D hourly measurements.....	60
Figure 23: Wind rose for TMY _{FR2} hourly measurements	61
Figure 24: Wind rose for TMY _{FR1} hourly measurements	61

List of Tables

Table 1: Cumulative Distribution Function of the sum of two dice	24
Table 2: Weight of parameters in the Sandia methods	27
Table 3: Weights for alternative selection for the Festa-Ratto method	31
Table 4: Statistics of some meteorological parameters for reference period 1991 - 2020 [47]	35
Table 5: List of parameters used by each method	39
Table 6: Limits for range and step tests and rate of data recovery	42
Table 7: Typical months by TMY method	43
Table 8: Monthly mean dry bulb temperatures ($^{\circ}\text{C}$) of TMY methods and long-term data	46
Table 9: Monthly maximum dry bulb temperatures ($^{\circ}\text{C}$) of TMY methods and long-term data	47
Table 10: Monthly mean wind speed (m s^{-1}) of TMY methods and long-term data	48
Table 11: Monthly sum of global solar radiation (KW h m^{-2}) of TMY methods and long-term data	49
Table 12: Dry bulb temperature percentage distribution for TMYs and long-term data ..	54
Table 13: Wind speed percentage distribution for TMYs and long-term data	55
Table 14: Global solar radiation percentage distribution for TMYs and long-term data ..	55
Table 15: Hourly dry bulb temperature ($^{\circ}\text{C}$) values by dataset and by probability of being recorded	63
Table 16: Hourly wind speed (m s^{-1}) values by dataset and by probability of being recorded	63
Table 17: Daily sum of global solar radiation (W h m^{-2}) values by dataset and by probability of being recorded	64
Table 18: Difference in CDF of hourly dry bulb temperature relative to long-term data by dataset and probability	65
Table 19: Difference in CDF of hourly wind speed relative to long-term data by dataset and probability	66
Table 20: Difference in CDF of daily sum of global solar radiation relative to long-term data by dataset and probability	67
Table 21: Sums of relative difference of each TMY using equal weights and modified weights	68

List of abbreviations

PPB	Parts per billion
TMY	Typical meteorological year
TSI	Total solar irradiance
TRY	Test reference year
EPS	Energy performance software
HVAC	Heating, ventilation and air conditioning
CFD	Cumulative distribution function
XMY	Extreme meteorological year
TMY _{S1}	Original Sandia National laboratories method
TMY _{S2}	Modified Sandia National laboratories method
TMY _D	Danish method.
TMY _{FR1}	Original Festa-Ratto method variant.
TMY _{FR2}	Modified Festa-Ratto method variant.

1 Introduction

1.1 Climate change: Evidence and Effects

Planet Earth is enclosed by the atmosphere, which is itself composed of several layers containing water vapour and other gases in varying amounts. The atmosphere starts at the surface of the Earth where the first layer is known as the troposphere, followed by the stratosphere, mesosphere, thermosphere and is lastly encapsulated by the exosphere, which ends 3,000 km away from Earth's surface. The atmosphere, especially the troposphere which spans 12 km above the surface, has played a crucial role in supporting the formation and sustenance of life on Earth by allowing it to retain part of the heat which is received from the sun. The layers of the atmosphere are illustrated in Figure 1.

The atmosphere contains radiatively active gases such as water vapour, carbon dioxide, ozone, methane and nitrous oxide; commonly referred to as "greenhouse" gases (GHG). By nature, the energy absorbed by the Earth has to balance the energy radiated from planet by releasing such energy as infrared radiation, also known as long-wave radiation. When long-wave radiation is emitted from the surface of the Earth, these gases absorb part of the radiation. Were it not for the presence of greenhouse gases surrounding Earth, the average temperature at the surface would be of -18°C , hence much colder than the current mean temperature of 15°C [1], [2]. The atmosphere allows approximately half of the solar radiation to penetrate to the Earth's surface, while the remaining 30% and 20% are reflected back and absorbed by the atmosphere, respectively. Thus, the atmosphere also acts as a shield against excessive solar radiation.

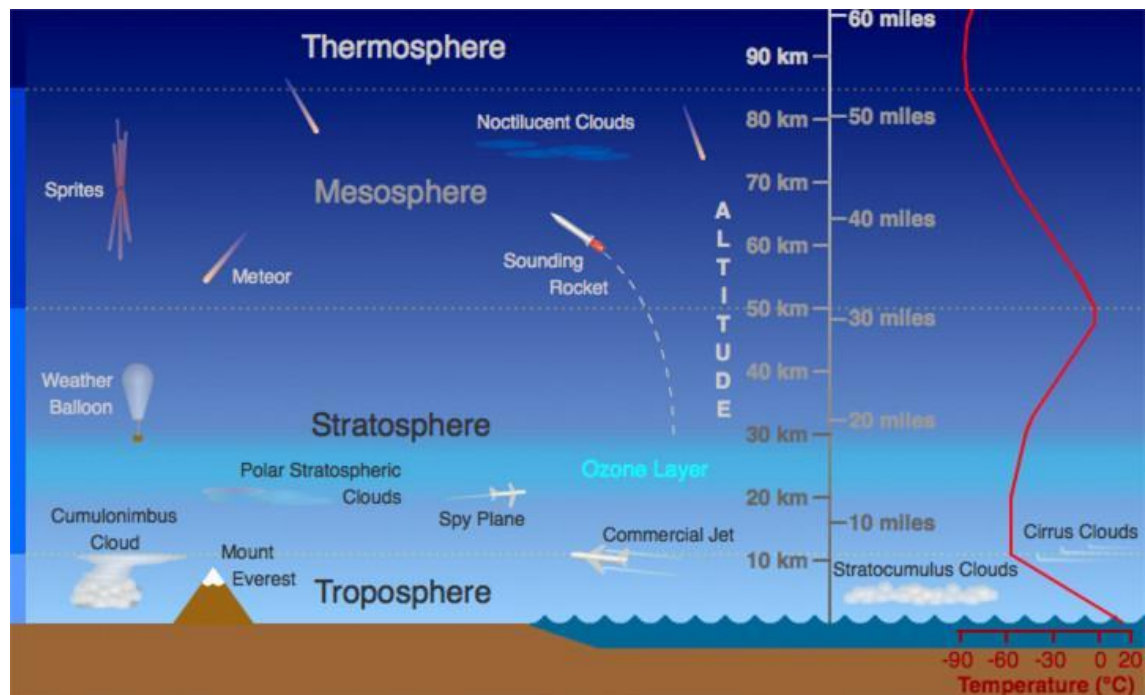


Figure 1: The layers of Earth's atmosphere [3]

The technological advances made by mankind led to the First and Second Industrial Revolutions, with the former commencing during the 18th century and the latter starting in the mid-19th century. These events brought about significant improvement in the standard of living and gradually reduced physical labour and expanded several economic activities thanks to newly-developed technologies. Such technologies were highly reliant on combustion of fossil fuels as a source of energy by converting the chemical energy into the mechanical energy required to power heavy machinery such as the steam engine and the internal combustion (IC) engine [4]. The combustion of fossil fuels such as coal, coke and petroleum products releases greenhouse gases and pollutants into the atmosphere.

As the Industrial Revolutions unfolded, the consumption of fossil fuels rose to unprecedented levels. Indeed, global emissions of carbon dioxide from fossil fuel combustion have been rapidly increasing since the second half of the 19th century, coinciding with the start of the second industrial revolution, with a mean year-on-year increase of 213.3 million tonnes of CO₂ [5].

Chapter 1: Introduction

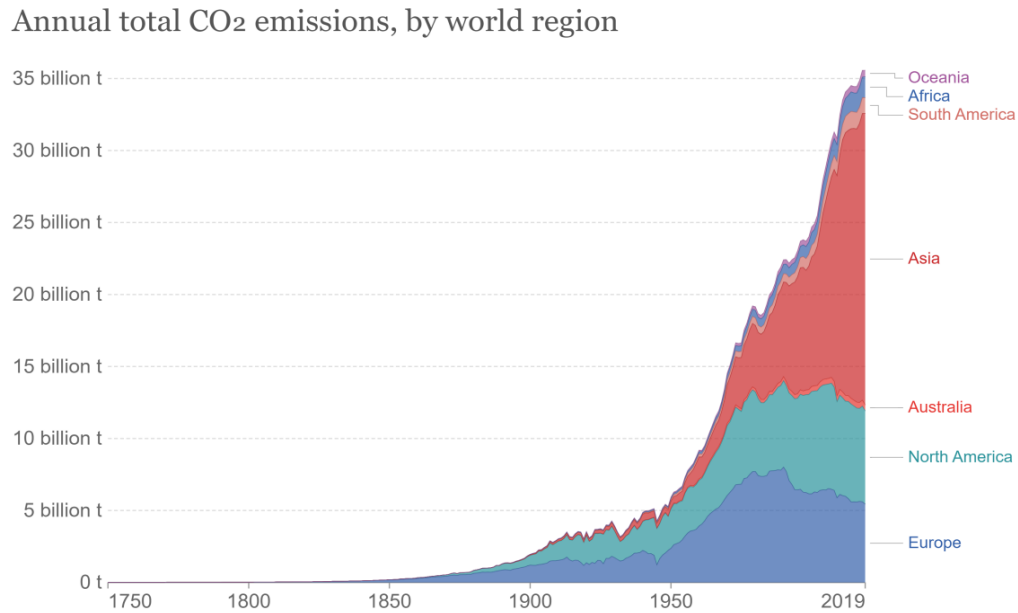


Figure 2: Global annual total CO₂ emission by continent over the period 1750 – 2019 [6]

These emissions are significant to the degree of disrupting the Earth's natural carbon cycle, whereby carbon dioxide is continually exchanged between the planet's surface and its atmosphere. Natural carbon sinks such as oceans, coastal vegetation and trees were able to capture most of the carbon emissions from sources such as agriculture, respiration of flora and fauna and natural waste. This cycle was a quasi-closed system prior to mankind's increased industrialisation. Increased human activity has altered the composition of the atmosphere, and carbon dioxide, methane, nitrous oxide and sulphur hexafluoride measurements at baseline conditions show that the proportion of these gases with respect to total atmospheric matter has been rising continually for as long as records have been kept. For example, the annual mean concentration of methane has risen from a value of 1644 ppb in 1984 to 1879 ppb in 2020, whereas for nitrous oxide, a concentration level of 316 ppb has increased to 333 ppb in 2020. Baseline measurements mean that the recorded concentrations are representative of background, or actual concentrations, as they are free from recent anthropogenic and natural occurrences [7], [8].

Chapter 1: Introduction

As described previously, the presence of these gases, which are radiatively active, increases the greenhouse effect. Although these gases have a relatively small contribution to the total tropospheric (and atmospheric) content in terms of mass or volume, it is their global warming potential which renders their presence dangerous. In fact, calculations based on air measurements show that the two most abundant gases are nitrogen and oxygen, which occupy 78.08% and 20.94% of the tropospheric volume, respectively. On the other hand, carbon dioxide, methane and nitrous oxide are trace gases and take up 0.036%, 0.00017% and 0.00003% of the volume [9].

The capability of a gas to contribute to the retention of heat within the atmosphere is known as its global warming potential (GWP). All greenhouse gases are compared to carbon dioxide, which has a GWP of 1, as a baseline. For example, methane and nitrous oxide have 100-year GWPs of 28 and 265 respectively. Fluorinated gases, or F-gases, which are used in the industrial sector as well as in cooling appliances as a replacement for ozone depleting substances, have a GWP which can reach values in the order of thousands [10]. In the EU, F-gas emissions peaked in 2014 at 107 million tons of CO₂ equivalent [11]. This shows that even though these percentages are very small, greenhouse gases can have a tremendous impact on the ability of the atmosphere to preserve heat received from the sun.

The increase of greenhouse gases in the atmosphere due to increase human activity has led to the well-known and globally recognised phenomenon known as climate change [12], [13]. Evidence from observations on ice cores and direct measurements show that carbon dioxide in the atmosphere has reached a level of concentration which is unprecedented in millennia; the level of 300 parts per million of CO₂ had never been reached before the 1950s and is currently in excess of 400 parts per million [14].

Climate change refers to a host of abnormal climate and weather observations, including increasing frequency and persistence of extreme weather conditions and of climatic parameters such as air and sea temperatures and precipitation. There are several indicators which demonstrate climate change. The global average temperature has increased by 1°C in 2020 when compared to the 1901 – 2000 long-

Chapter 1: Introduction

term average value. This quantity is known as the global temperature anomaly and was consistently below zero until the mid-20th Century [15].

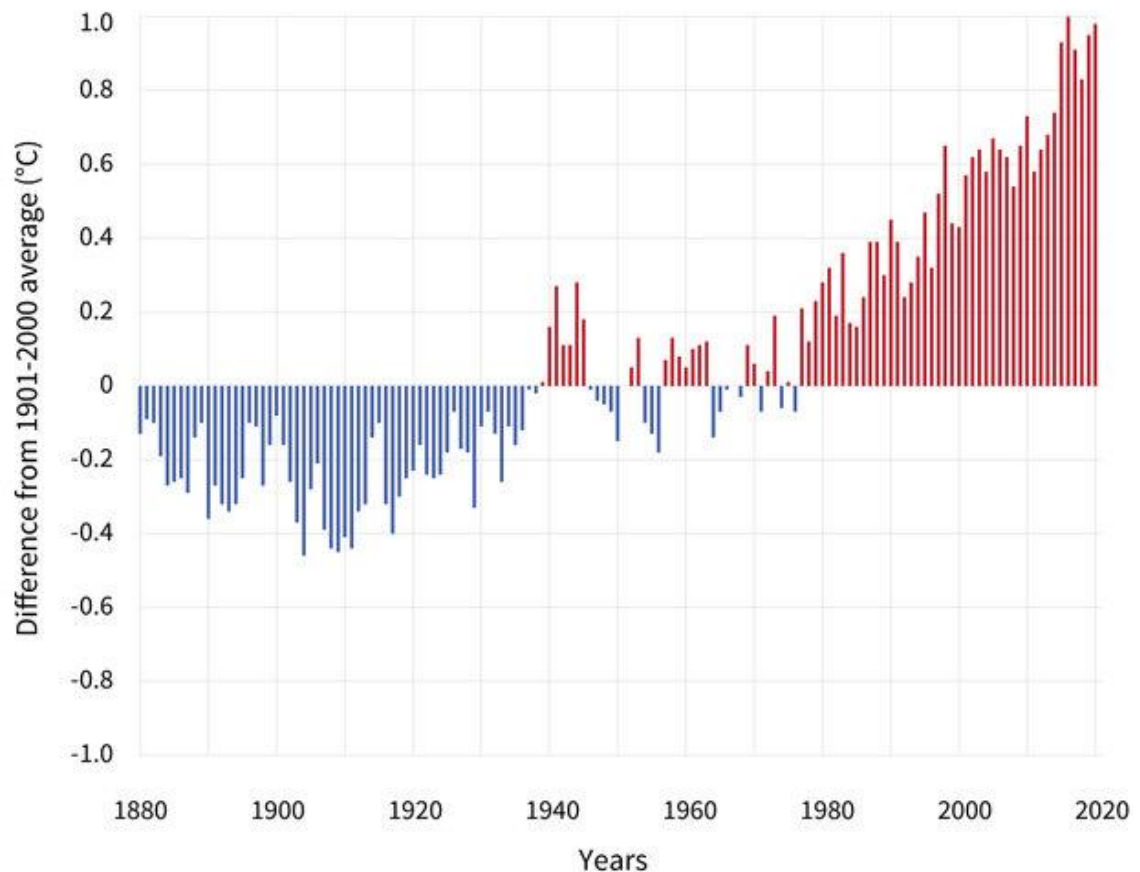


Figure 3: Global average surface temperature anomaly (1880 – 2020) [15]

This increase in surface temperatures has led to rising ocean temperatures as well since oceans and seas are the primary heat sinks of our planet. Rising temperatures have led to shrinking ice sheets, melting sea ice and glacial retreat. Because of these events, sea levels are rising along coasts of all continents. These changes in the natural environment do not only have direct consequences on local ecologies but also have repercussions which are felt all around the globe. For instance, the decrease in ice cover, both on land and at sea, has a multiplicative effect on the warming of the planet. Thanks to its white colour, ice sheets have a high albedo; in

Chapter 1: Introduction

other words ice cover serves as a highly reflective surface. The decrease in ice cover implies a reduction in the amount of reflected solar radiation, thereby increasing the radiation absorbed by the Earth and raising the globe's temperature. It is estimated that between 1992 and 2011, the ice sheets of Antarctica and Greenland have lost 1320 ± 980 and 2940 ± 940 Gt of ice respectively, which is equivalent to a global sea level increase of 11.1 ± 3.8 mm [16]. The melting of ice sheets has another significant impact on the greenhouse effect. Soils which have been frozen within the permafrost in very cold regions of the Earth become exposed to the air once the ice containing them melts. With the soil exposed, the previously trapped carbon dioxide and methane is released back into the atmosphere, thus contributing further to the greenhouse effect [17].

The decrease in the extent of sea ice is also detrimental to polar bears, which rely on the ice cover for resting and hunting. Polar bears, which are listed as a vulnerable species, are having to swim longer distances to find adequate ice to carry out their survival activities, thus wasting more energy and reducing their chances of finding seals to feed on, which greatly hinders their survival due to extended periods of fasting.

Global warming has also resulted in a significant increase in sea surface temperature. Indeed, the global sea surface temperature anomaly with respect to the 20th century was 0.77°C in 2019, whereas it had never exceeded zero between 1880 and 1940 and has been registering positive values ever since 1977 [18]. The oceans of planet Earth are important sinks of carbon dioxide. There are two main mechanisms by which oceans absorb carbon, namely by photosynthesis of phytoplankton and by direct chemical interaction. Similar to plants, phytoplankton have chlorophyll which enables them to collect incident solar radiation and convert it to chemical energy. During photosynthesis, phytoplankton absorbs carbon dioxide and releases oxygen as a by-product. Carbon dioxide also dissolves directly in water at the surface, hence the second uptake mechanism. As atmospheric CO_2 increases, so does the oceans' absorption of it to retain the carbon balance, meaning that the oceans' concentration of CO_2 is also steadily increasing and the oceans' ability to dissolve it is hindered. When ocean waters tend towards saturation, the rate of phytoplankton photosynthesis decreases, and this reduces CO_2 absorption

Chapter 1: Introduction

while also disrupting the entire marine food chain. In addition, the increased rate of CO₂ absorption acidifies the oceans posing further ecological risks [19].

As described previously, the evidence of climate change due to anthropogenic greenhouse gas emissions is substantial and agreed upon by the vast majority of scientists. With growing concerns over the Earth's future and well-being, scientists are dedicating more resources towards understanding the short-term and long-term consequences of global warming. Indeed, this phenomenon has far-reaching effects on the natural environment and long-established ecological processes which overarch with the well-being and quality of life of mankind.

Furthermore, increasingly anomalous weather patterns are being experienced all over the globe. Increasing temperatures are altering the water cycle, by which surface water from large water bodies evaporates and condenses and coupled with sublimated ice and snow, forms clouds which eventually build up, becoming heavy and saturated with water, which is followed by precipitation. As a result, rainfall intensity is increasing and periods of droughts and rainfall are becoming longer. Sea level is expected to continue to rise throughout this century, irrespective of any mitigation measures undertaken, putting coastal regions and low altitude areas at a much higher risk of severe flooding. The ocean will be negatively impacted from climate change due to higher heat content, leading to increased temperatures, reduced oxygen levels and higher acidity levels, thus disturbing vital ecosystems [20]. Changes in the natural environment are also impacting our daily lives. The increasing frequency of heatwaves, droughts and heavy rain are affecting quality of life as well as established activities, such as agriculture, which is important for both commercial entities, self-sustenance farms and for all consumers. Crop yields and soil properties will be affected due to longer periods of drought and more frequent extreme rainfall periods [21]. If fields are too wet before or during the time of sowing, then the planned crop will risk being lost. On the other hand, extended droughts are also unfavourable for many crops which require watering in areas where man-made irrigation methods are not common or relatively

Chapter 1: Introduction

expensive, or for families whose agricultural practices are purely for self-sustenance.

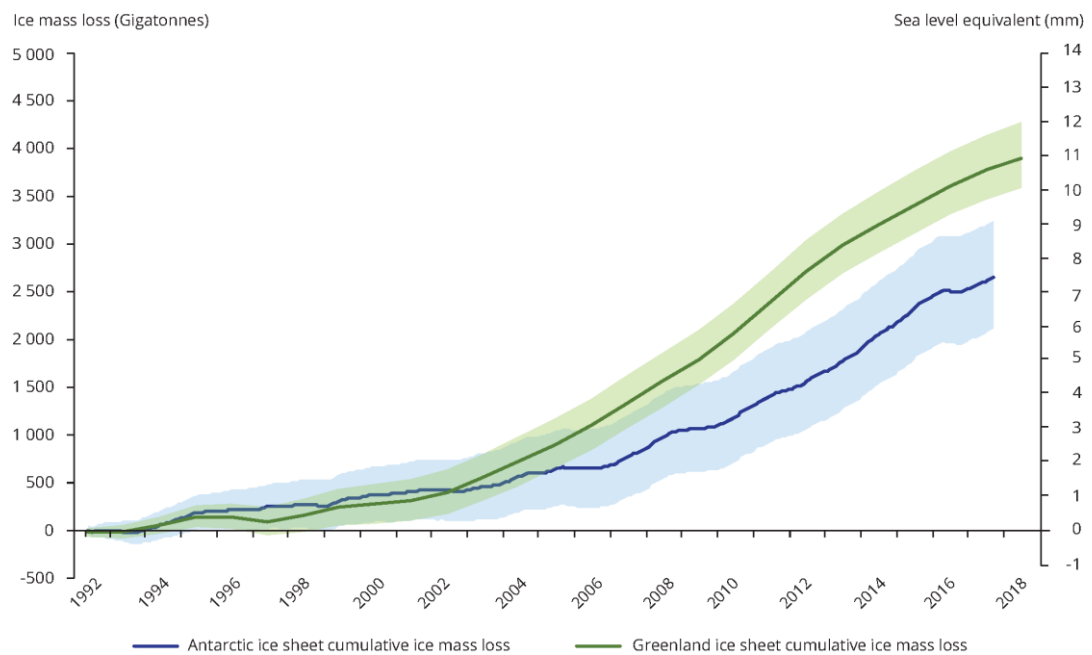


Figure 4: Cumulative ice mass loss from the Greenland and Antarctic ice sheets [22]

Climate change also has a range of consequences on both fossil fuels and renewable energy resources. For the former, the balance between the increasing pressure to reduce fossil fuel consumption and the need to generate the baseload energy demand consistently can destabilize energy markets and power plant projects. The current climate emergency has increased the demand for cleaner burning fuels and renewable energy, but further technological advances are required before certain fossil fuels can be completely phased out. On the other hand, the impact of climate change on renewables can be direct, due to the dependence on the climate's behaviour. For example, abnormal behaviour of the water cycle can have an effect on hydroelectric power generation and storage and consequently on the electricity supply of the reliant entities. There is also a secondary effect on renewable energy, due to increasing importance of green energy generation. For example, increased demand of silicon for applications in solar energy coupled with reduced supply from Chinese mines, from which most silicon originates [23], led to a 300%

Chapter 1: Introduction

increase in its price and a 400% increase in polysilicon used in solar panels in the space of two months [24]. This impacts solar energy technology prices, as well as costs of other industries where silicon is commonly used, such as the automotive industry for engine blocks. Such costs will be inevitably borne by producers and passed on to consumers. The increasing frequency of extreme weather as a result of climate change puts energy equipment and infrastructure, such as electricity lines, pylons, transformers as well as solar panels and wind turbines, at risk of being damaged, thus impinging on the reliability of energy supply.

1.2 Climate change mitigation

During the late 20th century the relation between climate change and increasing emissions and concentrations of greenhouse gases in the atmosphere due to human activity evolved from a mere notion to a concrete and acknowledged fact that has been gradually consolidated by scientists worldwide. In 1992 during the United Nations Conference on the Environment and Development, which was held in Rio de Janeiro, the United Nations Framework Convention on Climate Change (UNFCCC) was established in an effort to mitigate global warming. Between 1992 and 1997, the targets to be achieved were agreed upon and written up in the form of a protocol in Kyoto. The Kyoto protocol came into action in 2005 following a hefty ratification process. In the Protocol, countries are required to implement concrete mitigation measures and develop more environmentally-friendly policies to curb global warming. Currently, 192 parties are committed to the Kyoto Protocol.

One of the principal main aims of the Protocol was that parties reduce their average greenhouse gas emissions for the years 2008 to 2012 by 5% when compared to 1990 levels. The Protocol also introduced novel mechanisms for countries to reach the mentioned target, for example via emissions trading, where parties that did not exceed their emissions cap could “sell” their surplus allowance to others who would exceed theirs. The Kyoto Protocol entered a second commitment period extending up to 2020, but this phase saw a decrease in the number of parties

Chapter 1: Introduction

adhering to it and did not enter into force until 2020. On a different front sustained by the United Nations, an important and legally binding treaty, known as the Paris Climate Accords, was agreed upon and signed by 196 parties in between 2015 and 2016. The principal target of the Paris Agreement is to limit mean global increase in temperature to below 2°C when compared to the pre-industrial mean, while also making a significant effort to keep below 1.5°C. The progress towards the targets is reviewed every 5 years. Towards this goal, signatory parties had to submit their climate mitigation strategy, known as nationally determined contributions, outlining the measures and policies to be implemented. At the EU level, several regulations and directives have been created to boost the chances of reaching these targets. The most recent climatic venture is the EU Green Deal, a holistic set of proposals and commitments, targeting a 55% reduction of net greenhouse gas emissions in 2030 relative to 1990 emissions, and reaching net carbon neutrality by 2050.

It is clear that a huge global effort to mitigate climate change has been going on for many years, and that these efforts have had a positive impact on curbing global temperature increases. Part of the scientific community is dedicated to predicting the future climate based on different scenarios, policies and measures undertaken. This enables leaders and policy makers to take stock and to strategize.

In the IPCC Summary for Policymakers of 2021 [25], a number of scenarios of emission levels, formally known as Shared Socio-economic pathways (SSPs) and the resultant predicted temperature increases are presented. In the best case scenarios of reaching or approximating carbon neutrality by 2050 followed by net negative CO₂ emission, then the aforementioned temperature increase compared to pre-industrial levels will be of 1.5°C by 2040 and 1.6 to 1.7°C by 2060, depending on the rate of emissions reduction. The next best scenario is projected to produce a rise of 2°C by 2060. The worst case scenarios indicate a temperature increase of 2.1°C to 2.4°C by 2060. This analysis shows that if concrete action is taken and greenhouse gas emission levels remain in the same range as present, then the Paris Agreement target is achievable and if carbon neutrality is reached by 2050 then the ambitious 1.5°C limit will be within reach. Unfortunately these scenarios are optimistic and do not reflect the current state of affairs in terms of global

Chapter 1: Introduction

commitments to reduce emissions. Rather, with the present legislation and measures, the expected increase in temperature will probably be of 2.9°C, but can range between 2.1°C and 3.9°C [26]. It is clearer than ever before that we are in a crucial time to curb climate change and the permanent and irreversible consequences that could arise from it. A 1.2°C increase is already inevitable and humanity is currently in code red.

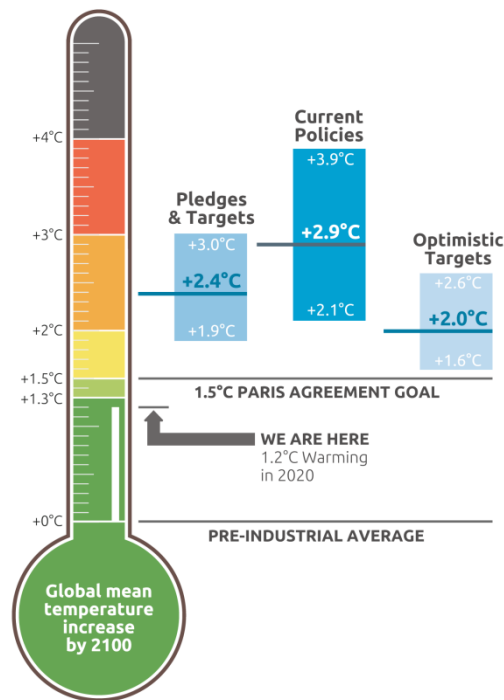


Figure 5: The Climate Action Tracker thermometer showing projected temperature increases by 2100 [21]

By studying the distribution of greenhouse gas emissions and energy use, world leaders become better equipped, enabling them to design policies and strategies to mitigate climate change and to work on the most emissions-heavy sectors. Global emissions data from the Climate Analysis Indicators tool (CAIT) [27] illustrated in Figure 6 shows that in 2018, the biggest sources of greenhouse gas emissions were electricity and heat generation, transport, manufacturing and construction and agriculture. Further insight on the sources of emissions can be drawn from historical trends of each sector. For example, emissions from electricity and heat

Chapter 1: Introduction

generation has increased from 8.6 Gt to 15.59 Gt of CO₂ equivalent from 1990 to 2019. Other sectors such as transport, manufacturing and energy use in buildings have also registered increases over the same time period, while other sector such as land use, waste and fugitive emissions have been relatively stable. This analysis shows that the technological advances which have led to more efficient technologies, renewable energy and end-of-pipe solutions have been outweighed by the increasing global population, improved standards of living and socio-economic growth and consumerism.

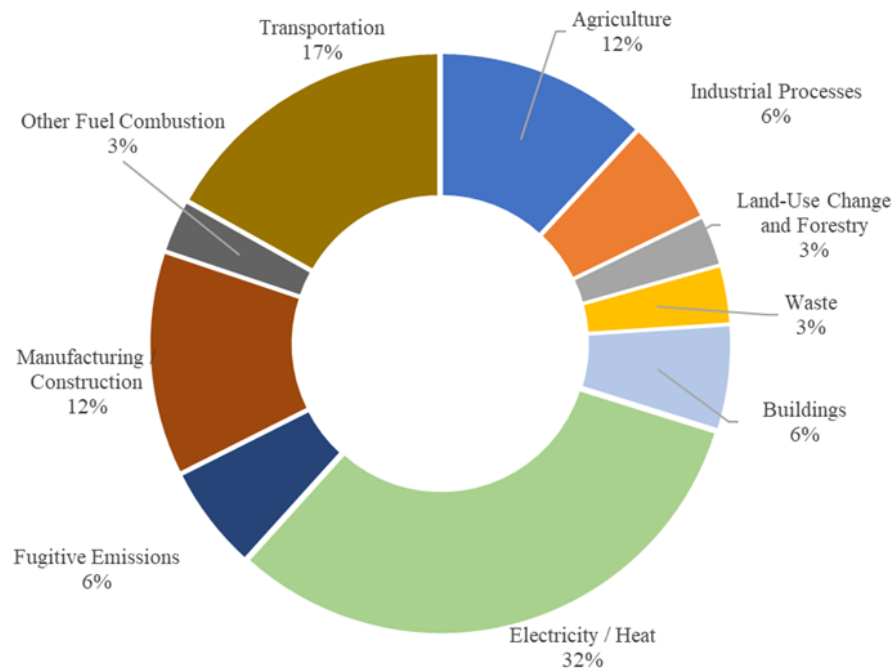


Figure 6: 2018 global GHG Emissions from CAIT data [23]

1.3 Energy performance of buildings

This dissertation focuses on the meteorological data applied to software used to model the energy consumption and efficiency in buildings. Part of global legislative efforts to mitigate climate change involve the design of more energy efficient

Chapter 1: Introduction

buildings by using the most suitable and cost-efficient materials and appliances for heating, cooling and lighting, amongst other items. The choice of such items depends on various properties such as the purpose, location, orientation and occupancy of the building.

In the EU, buildings account for 40% of the energy consumed [28]. At the level of the EU, the Energy Performance of Buildings Directive is the principal legislative tool whose aim is to record, measure, guide and regulate the design of buildings in terms of energy use. The first iteration of the Directive (2002/91/EC) required EU member states (MS) to set up methodologies for the calculation of the energy performance of buildings, the results of which are presented in the form of an energy performance certificate (EPC) indicating the average CO₂ emissions and related indicators. The EPC shall be presented to the buyer or tenant prior to the sale or rental of a property. The Directive also guided MS to set up minimum energy requirements for new buildings and for existing ones with a floor area exceeding 1000 m². The Directive was recast into Directive 2010/31/EU and introduced new guidelines. For example, it requested that building design and retro-fitting is oriented towards cost-optimal efficiency.

The concept of “Nearly zero energy buildings (NZEB)”, i.e. buildings whose net energy use is close to null, was introduced and required for all new buildings built after 31st December 2020 and after 31st December 2018 for buildings occupied by public authorities. This was to be accompanied by a concrete plan as to how the MS shall achieve a significant increase of NZEBs. MSs were urged to provide financial incentives and other measures to promote more optimal technologies and materials in building design. The EPC was amended by including the most economically and technically feasible improvements.

Furthermore, with the latest recast for this EPBD (EU) 2018/844, MSs are to provide long-term renovation strategies based on the current building stock, targeting residential and non-residential buildings, promoting deep and cost-effective renovations. The directive introduced the concept of a building renovation passport, i.e. a long-term, step-by-step renovation roadmap to increase its energy performance based on an on-site energy audit. The Directive also

Chapter 1: Introduction

requires the regular inspection of heating and air-conditioning systems exceeding a certain output threshold. In the EU Green Deal, the focus is on starting a so-called “Renovation Wave”, increasing climate-proofing of buildings and enhancing the enforcement of energy performance rules.

Another important legislative tool is Directive 2012/27/EU on energy efficiency, whereby MSs are encouraged to develop building renovation strategies with energy efficiency in mind, by taking stock of the building population, earmarking cost-efficient and energy saving renovations and developing appropriate policies and structures. The Directive also regulates energy efficiency in the supply phase. This Directive was also reviewed and a new recast (EU) 2018/2002 was issued to be in line with the EU’s 2030 targets of reducing emissions by 40% compared to 1990 levels, reaching 32% renewable energy sourcing and raising energy efficiency to 32.5%.

Different software packages that model the energy performance of buildings exist and are selected according to the type of building at hand. The use of local meteorological data are important parameters in such simulations. However, a set of meteorological data representing the Maltese Islands’ typical weather conditions applicable to modelling software is not yet available. This is the motivation for this study, i.e. to obtain a comprehensive hourly dataset in the form of a typical meteorological year (TMY). As is explained in detail in the following chapter, a TMY is based on a multi-year time series of meteorological parameters and their derivatives, which considers the solar cycle of approximately 11 years, during which period the sun’s activity and output undergoes several variations. Furthermore, the TMY is not an average, but contains actual historical data which is selected using statistical comparison tests that determine the months most typical from the set of available months being investigated.

1.4 Objectives and structure

This dissertation aims to produce a set of TMYs based on different statistical methods presented in literature. This involves the application of several statistical

Chapter 1: Introduction

tools to determine which month is the most typical from all those available. The TMY methodologies will be applied to the hourly data provided by the Malta Meteorological Office and supplemented by solar radiation data from the Institute for Sustainable Energy. The methodologies vary in terms of the meteorological parameters considered, the statistical tools used and the final selection criteria of the candidate months. The TMYs were produced using Microsoft Excel version 2108.

Another objective of this dissertation is to investigate the TMYs produced by analysing the resultant climatic behaviour and distributions. This analysis will also enable a cross-comparison of the TMYs, which will help identify the different characteristics, as well as those in common, which were captured by the different methodologies.

The final goal of this dissertation involves the selection of the most appropriate TMY to be applied in energy performance modelling software. This will be based on the outcome of the previous objectives which will provide several indicators from each TMY produced. In cases where consecutive months are chosen from different years, smoothing of weather parameters in their transition from the last day of one month to the first day of the next month is required, given that these months will be chosen as candidate months for the TMY from different years. The smoothing across the transition between months ensures the continuity of the respective meteorological parameters and eliminates unnatural jumps of the measurements.

Chapter 2 presents the literature review. In this chapter, the scientific research related to this dissertation is presented. It mainly focuses on the solar cycle, the statistical tests and mathematical formulae utilized in the development of TMYs and the TMY methodologies which have been implemented in this dissertation. The processes behind each TMY are presented in full detail. The chapter also presents salient points on the climate of the Maltese Islands.

In Chapter 3, the methodology implemented in this dissertation is presented. The chapter focuses on the data preparation and treatment applied before and during the production of the TMYs.

Chapter 1: Introduction

Chapter 4 presents the results obtained. The primary results obtained are the set of five hourly meteorological datasets spanning the calendar year, based on the typical meteorological months chosen to form the different TMYs based on the relevant methodology applied to the original dataset. The chapter includes cross comparisons between the resultant TMYs, based on the behaviour of meteorological parameters.

Chapter 5 contains the conclusions of the dissertation and presents a reflection on this dissertation and its outputs. A number of recommendations for future work related to this subject are presented as well.

2 Literature Review

2.1 Introduction

A typical meteorological year (TMY) forms the basis for accurately modelling the energy performance of buildings, which is currently being given utmost attention at EU and international levels, in a bid to achieve carbon neutrality by 2050. A representative hourly dataset of meteorological parameters is required in order to calculate heat gains and losses throughout the building envelope, to study the efficacy of passive heating and cooling methods and to determine the energy consumption of active HVAC systems to maintain temperature levels according to the building's requirements and to achieve thermal comfort. Such data is also useful for the calculation of energy yield and cost savings derived from renewable energy systems.

A TMY should reflect the most common climatic observations over a long period of time. This is carried out by the collation of the most typical months within at least an 11-year consecutive period, which covers the period of one solar magnetic activity cycle. The statistical methods used to produce a TMY are presented in this chapter.

2.2 The Solar Cycle

Quasi-periodically the sun undergoes a cycle of maximum and minimum solar activity and fluctuating levels of activity in between in an approximately sinusoidal curve. The solar cycle is governed by the magnetic activity of the sun, whose variation is caused by the fact that the period of rotation of the sun varies along different lines of latitude, going from 25 days at the equator to 35 days closer to the poles. This phenomenon is known as differential rotation and occurs because of the convection of matter occurring inside the sun close to its outermost layer. The convection of matter within the sun is enabled by the extremely high temperatures

Chapter 2: Literature Review

in this convective zone, which consists of solar plasma. Plasma is a state of matter similar to a gas, but which has a net non-zero charge due to free-flowing electrons and positive ions. As such, the charged solar matter which is in motion in the convective layer generates the magnetic field of the sun. Figure 7 shows a coronal loop emerging from a pair of sunspots on the surface of the sun. The sun's strong magnetic fields break out from below the photosphere and become visible as the magnetic field arcs between the sunspot pair. This is an example of how the presence of sunspots alters the behaviour of the sun's photosphere and causing variations in its irradiance.



Figure 7: A coronal loop emerging from a pair of sunspots [29]

The rates of rotation of the sun at different latitudes are determined by observing the rotation of sunspots at those latitudes on the sun's surface relative to background stars. Differential rotation produces twists in the sun's magnetic field lines, hence varying the magnetic activity, and this serves to flip the magnetic poles every 11 years [29].

Solar activity is measured by observing sunspots on the surface of the sun. Sunspots are the manifestation of highly concentrated magnetic activity in the form of energy displacement from the sun's surface. Events such as solar flares and coronal mass ejections are the result of sunspots. Sunspots have been observed since the early 17th century, whereas the solar cycle was discovered in 1843. The

Chapter 2: Literature Review

last completed cycle peaked at 129 sunspots in April of 2014 [30]. Incidentally, it was through the observation of sunspots and their rotation that led to the discovery of the sun's differential rotation. The current solar cycle started towards the end 2019 and is the 25th observed cycle.

A study based on meteorological data obtained by the Nimbus 7 satellite showed that the variation in total solar irradiance (TSI) follows the variation in the number of sunspots in a periodic cycle [31]. This relationship between TSI and sunspot numbers is illustrated in Figure 8, where solar irradiance and sunspot number change both follow a sinusoidal pattern and are in synchronisation with one another. The peak sunspot activity coincides with the flipping of the magnetic poles. However, solar cycles are dynamic and the peak number of sunspots as well as the peak solar irradiance are not the same across cycles. Specifically, the maximum number of sunspots in solar cycle 22 was 214, while solar cycle 23 experienced a maximum 180 sunspots and solar cycle 34 experienced a maximum of 116. Another interesting facet of solar cycles is that the sun can undergo consecutive cycles where the solar irradiance is significantly higher or lower than the typical levels. For example, the Maunder minimum was a period roughly between 1645 and 1710 during which sunspot numbers were much lower than usual and solar irradiance was also very low, with conservative models yielding a maximum of 15 sunspots per day [32].

In contrast, the Modern Maximum, which started in 1914, exhibited relatively high solar activity when compared to previous periods. The Modern Maximum is considered to have ended at the end of solar cycle 23 in the year 2000, due to the fact that solar cycle 24 has shown average solar activity [33]. During this period, in solar cycle 19, a maximum sunspot number at one point was 285, whereas in this cycle a daily average of 129 sunspots was observed.

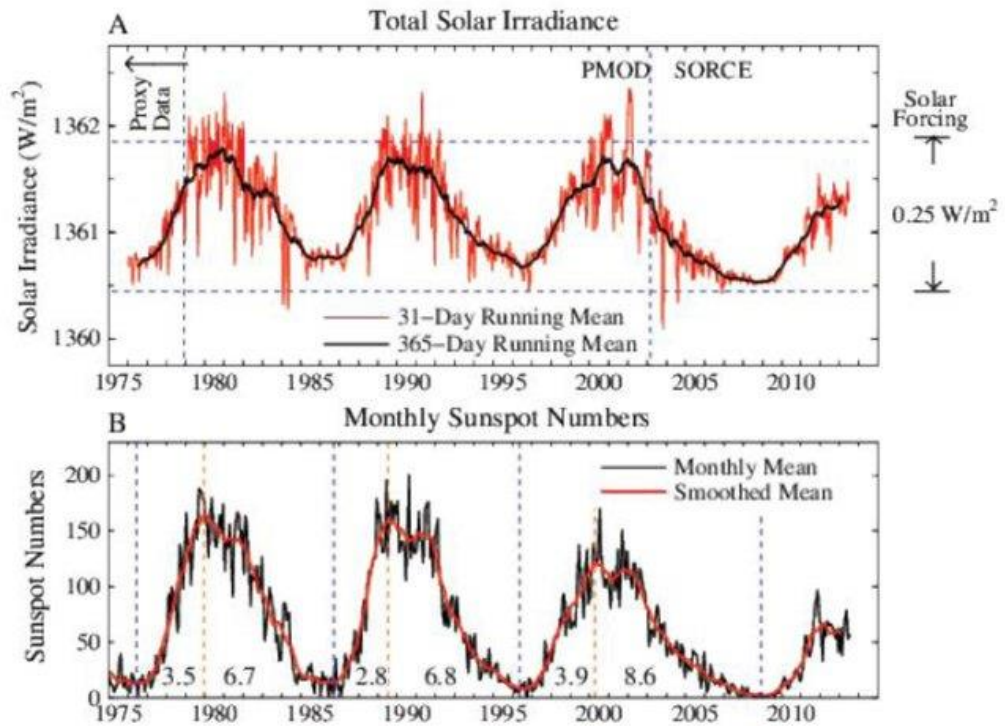


Figure 8: Solar irradiance and sunspot number in the era of satellite data [31]

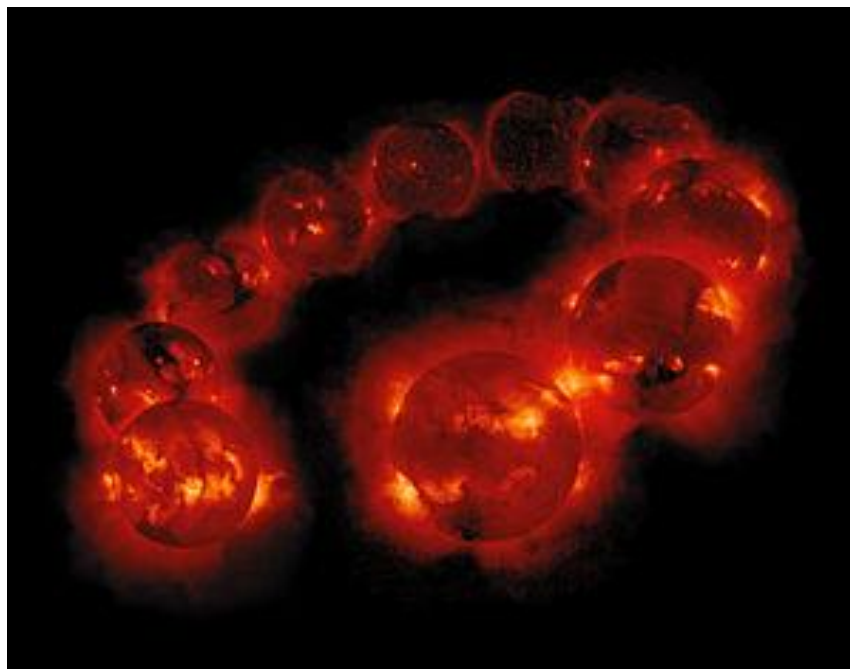


Figure 9: A montage of images of the sun spanning between 1991 and 2001 obtained from the Yohkoh solar observatory spacecraft [31]

Chapter 2: Literature Review

The variation of energy coming from the sun has led to debate regarding the effect of the solar cycle on global warming, and whether this cycle is the primary cause for increased global temperatures. Indeed, the impact, if any, of solar irradiance dynamics on climate change has been the subject of several studies. The empirical analysis carried out by Scafetta in 2009 on climate models showed that the contribution of changes in solar irradiance on global temperatures cannot be determined with certainty, due to a range of composites of TSI satellite measurements. When modelling global temperatures on the basis of these measurements, the global warming due to solar irradiance could be negative as well as positive, i.e. there is a very large uncertainty [34].

A study based on several global temperature datasets found that the sun's 11-year cycle was undetectable throughout most of the globe, whereas it was affecting very particular locations, namely the segments located in the 10° latitude interval of the tropics within the Pacific Ocean [35]. Furthermore, scientists are able to calculate the forcing, i.e. the contribution to global warming, of a particular phenomenon. It is estimated that the forcing due to changes in solar irradiance between 2000 and 2010 was -0.12 W/m^2 , where the negative sign implies that a cooling effect was produced, compared to the GHG forcing of 3 W/m^2 [36].

2.3 Typical Meteorological Year (TMY) – Definition and Methods

Energy performance software (EPS) accurately calculates the energy consumption and efficiency of a building, based on the building's physical characteristics which impinge on energy use. Furthermore, certain EPSs provide insight as to the expected energy consumption patterns with respect to the time of day and month of the year. The EPSs may also provide energy consumption trends according to where the energy was needed, such as in the form of water heating, lighting, space cooling and space heating. Such software require an hourly dataset of the most important meteorological parameters, spanning the entire calendar year. The quality of this dataset is of paramount importance to ensure that the outcome results generated by the EPS are realistic.

Chapter 2: Literature Review

There are different ways to obtain this meteorological dataset. One of the earliest datasets of this kind was the Typical Reference Year (TRY). The TRY was obtained by a selection process based on the years 1948 – 1975. The selection process was carried out by iteratively eliminating years where the dry-bulb temperature was extremely low or high. This resulting in one actual year being selected as representative [37]. The simplistic approach of this method yields a year which is void of extreme dry-bulb temperatures, hence narrowing down the temperature ranges to the best-case scenarios. Furthermore, this method places no importance on other meteorological parameters, such as global and diffuse solar irradiance, wind speed and direction and humidity.

A more representative dataset for use in EPSs is called the Typical Meteorological Year (TMY). A TMY consists of actual data, wherein each month is selected from a multi-year dataset. The most representative month is selected from all the available months using statistical methods which determine the most typical one. Therefore, a TMY will consist of 12 months, possibly from different years, which are concatenated to form a complete hourly dataset. The fact that a TMY contains actual data makes its use advantageous compared to using an averaged dataset. This is because, when taking an average of a parameter, the extreme values are eliminated. Moreover, it may be argued that, using a dataset composed of meteorological parameters covering a multiple-year span, makes EPSs generate a much more representative output when compared to using a TRY.

Although this is entirely plausible, the computational effort required if a multi-year dataset is used would be significantly higher, and perhaps not feasible, or not worth the marginal improvement over the result generated when using a TRY. The timespan which the base dataset used to develop a TMY covers can vary depending on the availability of data records and of the individual parameters. Indeed, different methodologies which are used to derive TMYs do not use a common set of parameters.

It is worth pointing out that in other studies, different lengths of time have been used. For example, the first TMY produced for Athens, Greece, utilised a 17-year dataset [38]. A different study in Spain produced two TMYs for the cities of Madrid

Chapter 2: Literature Review

and Valladolid, and the base datasets spanned 24 and 10 years respectively [39]. Therefore, there is no hard and fast rule as to the exact number of years needed to derive a TMY, although a minimum of 8 years is required to describe truthfully the long-term climate characteristics [40].

2.3.1 Statistical tools

There are several different methods to determine a TMY from a multi-annual dataset. Each method is basically a selection algorithm based on statistical tests and measures. The following are the statistical tools which are important for the forthcoming methods:

- Cumulative Distribution Function

The cumulative distribution function (CDF) of a real-valued random variable X is a function which, at a value x , gives the probability that the random variable X has a value which is less than or equal to x , as given by the equation below:

$$\text{CDF}_X(x) = P(X \leq x) \qquad \text{Equation 1}$$

For example, consider two dice being rolled and let the random variable X be the sum of the numbers on the two dice. Then, the values of the CDF, calculated using Equation 1, are tabulated in Table 1.

Table 1: Cumulative Distribution Function of the sum of two dice

x	$P(X = x)$	$CDF_x(x)$
2	1/36	0.028
3	2/36	0.083
4	4/36	0.194
5	6/36	0.361
6	6/36	0.528
7	6/36	0.694
8	4/36	0.806
9	2/36	0.861
10	2/36	0.917
11	2/36	0.972
12	1/36	1

In cases where the CDF is to be calculated for a sample dataset of size n , such as the meteorological dataset on which this dissertation is based, then the CDF is equivalent to the empirical distribution function which, for any value x , is given by Equation 4.

- Finkelstein-Schafer Statistic

The Finkelstein-Schafer (FS) statistic, calculated for a particular month m and year y , is mathematically defined by the following equation:

$$FS_x(y, m) = \frac{1}{n} \sum_{i=1}^n |CDF_m(x_i) - CDF_{m,y}(x_i)| \quad \text{Equation 2}$$

where x is the value of a random variable and n is the number of observations in the month m . The CDF_m is the long-term cumulative distribution function of month m and parameter x .

Chapter 2: Literature Review

- Weighted Sum of Finkelstein-Schafer Statistic

The weighted sum of the FS statistic, which can be calculated for any particular month, is defined as follows:

$$WS(y, m) = \frac{1}{M} \sum_{x=1}^M WF_x \cdot FS_x(y, m) \quad \text{Equation 3}$$

where M is the set of all parameters being considered and WF is the weighting factor which is assigned to each parameter.

- Kolmogorov-Smirnov Test

The Kolmogorov-Smirnov (KS) test compares the CDF with the sample CDF, also known as the empirical CDF, of a probability distribution. The KS statistic is calculated for a particular CDF with a two-step procedure as follows. First, the empirical distribution function of a set X of n independent and identically distributed observations, defined by the below equation, is calculated:

$$S(x) = \frac{\text{number of elements in sample} \leq x}{n} \quad \text{Equation 4}$$

Then, the KS statistic is given by the following equation:

$$KS(X) = \sup_x |S(x) - CDF_X(x)| \quad \text{Equation 5}$$

where \sup_x is the smallest possible upper bound of all the absolute value of the differences between the empirical distribution function and cumulative

Chapter 2: Literature Review

distribution function of x , where x takes values across X . Note that for a sample dataset, n represents the size of the sample.

- Percentile

A percentile is a statistical measure indicating the percentage of all observations which fall below a certain value. For example, the 50th percentile is the observation value below which 50% of all observations fall. As a practical example, consider a class exam where students can score a mark from 0 to 100. Then, if the mark of 75 is at the 90th percentile, this implies that 90% of the students obtained a mark which is strictly less than 75. This is the exclusive definition of a percentile. On the other hand, the inclusive definition states that the percentile includes the value at which that percentile is being calculated. For example, the 50th percentile is the value at or below which 50% of all observations fall.

- Standard Deviation

The standard deviation σ is a measure which indicates the dispersion of a set of values with respect to their mean. A large standard deviation indicates that values are significantly varied above and below the mean, whereas a small standard deviation signifies that values are relatively close to the mean.

2.3.2 TMY Methods

The description of a number of TMY methodologies is presented below.

2.3.2.1 The Sandia National Laboratories Method

The Sandia National Laboratories Method determines the TMY based on 9 parameters, namely the mean, minimum and maximum dry bulb temperature (\bar{T} , T_{\min} , T_{\max}) and relative humidity (\overline{RH} , RH_{\min} , RH_{\max}) mean and maximum wind

Chapter 2: Literature Review

speed (\bar{W} , W_{\max}) and total horizontal solar radiation (G). The afore-mentioned variables are weighted as follows:

Table 2: Weight of parameters in the Sandia methods

Parameter	TMY _{S1} weights	TMY _{S2} Weights
Mean dry bulb temperature	2/24	2/20
Maximum dry bulb temperature	1/24	1/20
Minimum dry bulb temperature	1/24	1/20
Mean relative humidity	2/24	2/20
Maximum relative humidity	1/24	1/20
Minimum relative humidity	1/24	1/20
Mean wind speed	2/24	1/20
Maximum wind speed	2/24	1/20
Global solar radiation	12/24	5/20
Direct solar radiation	0	5/20

The weighted sum of the FS statistic of the 9 parameters is calculated for each month in the time series and for each calendar month and the 5 months having the smallest weighted sum are selected, while the rest are eliminated. This is calculated by using Equation 2 and Equation 3. The weighting factors used to calculate Equation 3 are provided in Table 2.

Then, the five candidate months are ranked according to their closeness to the long-term mean and median of both the dry bulb temperature and the global horizontal solar radiation. These four values are calculated for each candidate month as well as for the respective months over the entire time series, the latter giving the long-term value. For each candidate month, the absolute differences between that month's value and the long-term value are calculated, and the maximum of these four differences is assigned to each month.

Chapter 2: Literature Review

Further selection is achieved by determining the frequency and the number of consecutive days, i.e. run length which each candidate month exhibits outside certain limits defined by fixed long-term percentiles. The lower and upper limit for dry bulb temperature are set to be the 33rd and the 67th long-term percentiles. For global solar radiation, only a lower limit, set to be the 33rd percentile, is defined. The month with the longest run, the month with the most runs and the month with zero runs are all eliminated. From the two remaining candidate months, the month ranking highest according to the previous step is selected as the month to form part of the TMY [38], [41]. This method will be labelled TMY_{S1}. The Sandia method has been incorporated in a number of studies and TMY generation projects, where authors have modified the weighting factor of the parameters in Table 2, as well as added new parameters [42]. One variant of this method which is of particular interest for this dissertation is called the TMY2 method, which was developed to accommodate the requirement to account for direct solar radiation, which was not included in the original Sandia method [43]. The weighting factors are presented in Table 2. This method will be labelled TMY_{S2}.

2.3.2.2 The Danish Method

The Danish method, also based on several steps, qualifies candidate months using the following parameters: mean and maximum dry bulb temperature, relative humidity, wind speed, atmospheric pressure, sunlight duration and global horizontal solar radiation. For each parameter, if the mean value of the candidate month is more than one standard deviation away from the long-term mean of the respective month, then the month scores zero, otherwise the month scores one. The final score of each month is the sum of scores from each parameter. Therefore, each individual month can have a score ranging between zero and seven.

In this step, the hourly meteorological readings are converted into daily residuals with respect to the smoothed daily long-term values. The parameters considered are the daily mean temperature, daily maximum temperature and daily sum of global solar radiation. This is done by means of the following equation:

$$Y(y, m, d) = x(y, m, d) - \mu_x(m, d) \quad \text{Equation 6}$$

where, $x(y, m, d)$ is the daily parameter, $\mu_x(m, d)$ is the long-term mean of the parameter and $Y(y, m, d)$ is the residual of the parameter $x(y, m, d)$. Following this, the standardized mean, $f_\mu(y, m)$, and standardized standard deviation, $f_\sigma(y, m)$, of each residual are calculated, as given by the following equations:

$$f_\mu(y, m) = \left| \frac{\mu_Y(y, m) - \mu_{\mu_Y}(y, m)}{\sigma_{\mu_Y}(y, m)} \right| \quad \text{Equation 7}$$

$$f_\sigma(y, m) = \left| \frac{\sigma_Y(y, m) - \mu_{\sigma_Y}(y, m)}{\sigma_{\sigma_Y}(y, m)} \right| \quad \text{Equation 8}$$

where $\mu_Y(y, m)$ and $\sigma_Y(y, m)$ are the mean and standard deviation of the residual $Y(y, m, d)$ over the candidate month respectively, $\mu_{\mu_Y}(y, m)$ and $\mu_{\sigma_Y}(y, m)$ are the means of $\mu_Y(y, m)$ and $\sigma_Y(y, m)$ respectively and $\sigma_{\mu_Y}(y, m)$ and $\sigma_{\sigma_Y}(y, m)$ are the standard deviations of $\mu_Y(y, m)$ and $\sigma_Y(y, m)$ respectively. Therefore, each candidate month will have three standardized means and three standardized standard deviations; one for each parameter. For each candidate month, the maximum of these six parameters is labelled $f_{\max}(y, m)$ and assigned to it. For each calendar month, the three months with the smallest $f_{\max}(y, m)$ are selected as candidate months, with the rest being removed. Finally, the months with the highest score as determined by the first step are selected to form part of the TMY [38]. This method will be labelled TMY_D.

Chapter 2: Literature Review

2.3.2.3 The Festa-Ratto method

The Festa-Ratto method builds on the Danish method but comprises more advanced statistical treatment. The standardised residuals with respect to the long-term data are calculated as follows:

$$X(y, m, d) = \frac{x(y, m, d) - \mu_x(y, m, d)}{\sigma_x(y, m, d)} \quad \text{Equation 9}$$

where $X(y, m, d)$ is the standardised residual of the parameter $x(y, m, d)$ with respect to the smoothed mean and standard deviation. Then, the first order products of the standardised residuals are calculated and converted into first order products' standardised residuals with respect to the long-term data on a daily basis:

$$z(y, m, d) = X(y, m, d) \cdot X(y, m, d + 1) \quad \text{Equation 10}$$

$$Z(y, m, d) = \frac{z(y, m, d) - \mu_z(m, d)}{\sigma_z(m, d)} \quad \text{Equation 11}$$

where $Z(y, m, d)$ is the standardized residual of the first order product parameter $z(y, m, d)$ for each specific day d of month m and year y , with respect to the smoothed mean and standard deviation $\mu_z(m, d)$ and $\sigma_z(m, d)$ respectively.

For each X and Z parameter calculated above, the mean, standard deviation and cumulative distribution are calculated for each individual month (short-term) and for the 12 months in the long term. The differences between the short-term and long-term means and standard deviations, namely d_{av} and d_{sd} , as well as the Kolmogorov-Smirnov statistic, d_{KS} are calculated. This yields six distances, two groups of three for each parameter X and Z . For each of these groups, a composite distance is calculated using Equation 12.

$$d(y, m, j) = (1 - a - b) \cdot d_{KS}(y, m, j) + a \cdot d_{av}(y, m, j) + b \cdot d_{SD}(y, m, j) \quad \text{Equation 12}$$

in which $a = b = 0.1$ are constants and j represents X and Z.

For each individual month, these two distances are calculated for the daily mean and maximum air temperature, mean relative humidity, mean wind speed and daily sum of global solar radiation, thus producing 10 distances for each individual month. Lastly, the maximum of these 10 distances is assigned to each candidate month, and the month with the smallest maximum is chosen as the month to form part of the TMY. This method will be labelled TMY_{FR1} . Alternatively, the final selection can be based on a weighted sum of the 10 distances, weighted according to Table 3 below [38] and will be labelled as TMY_{FR2} .

Table 3: Weights for alternative selection for the Festa-Ratto method

T_{\max}	\bar{T}	\overline{RH}	\bar{W}	G
1.0	2.0	1.0	1.0	5.0

The list of methods presented in this section is not exhaustive. The methods described can be arbitrarily varied through changes in weighting factors and final selection steps. However, from literature which was consulted for this current dissertation, the three methods described above were the most commonly used in other projects and are considered the most suitable, while still providing an array of TMYs for final analysis. The selected methods are also reasonably varied in terms of statistical tests and final candidate selection techniques. Other unique methods for the generation of the TMY exist. One example is the EN ISO 15297-4:2005 technical standard. This method shares similarities with the Sandia method, but the final selection process is based solely on the candidate months' absolute deviation from the long-term mean wind speed [37]. Hence, this method was not considered for this dissertation.

Although TMY methods mentioned use different statistical tools, each one uses these tools as a measure of each month's discrepancy from the long-term mean of the calendar month, and tends to select the month which, to an extent, resembles

Chapter 2: Literature Review

most the average behaviour across the time-span in consideration. For example, in the first step of the Danish method, parameters whose mean of a particular month is less than one standard deviation away from the long-term mean raise the score of that month and increase its chances of being selected for the TMY. This implies that months with relatively less frequent extreme behaviour have a stronger candidacy. Therefore, this could result in the TMY to be constructed in such a way that extreme measurements are excluded or scarce. If extreme meteorological conditions are excluded, this can skew the results of building energy simulations as the simulations would be carried out only in mild conditions closer to the average.

In light of this, a study published in 2015 [44] presented a modified approach, termed as the Extreme Meteorological Year (XMY). To determine the XMY, the months are chosen based on the parameters of dry-bulb temperature, dew-point temperature, solar irradiance, relative humidity and wind speed. Months may be selected based on two criteria; daily extremes and hourly extremes. For a particular parameter, daily extreme months are those months with the most extreme value of that parameter. In other words, the months with the highest and lowest value of a particular parameter are chosen. Daily extreme months are those months which, for a particular parameter, the month/s with the most extreme values, i.e. the minimum and maximum extremes, are selected. For the same parameters, hourly extreme months are those months whose average hourly values over the entire month are the most extreme. The minimum extreme months are not applicable for solar irradiance due to the fact that this parameter reaches zero during each day. It is clear that the XMY methodology is rudimentary in comparison to the TMY methodologies, and its results will not be considered for the final TMY selection. Nevertheless, it can serve as a reference to investigate whether extreme climatological behaviour is still captured in the various TMY methods.

Another important aspect to consider when deriving the TMY is the assembly of the different months. In the instances where two consecutive months of a TMY have been extracted from two different years, a discontinuity would arise in the adjacent days of the two months. To smoothen the transition between these two days, the

last 6 hours of the first day and first 6 hours of the first day are interpolated. Smoothing is not required for solar radiation due to the natural night-time transition where the value goes to zero. Smoothing is achieved by means of interpolation [37].

2.4 Characteristics of the Maltese Climate

Generally, the Maltese climate is characterized by hot, dry summers and mild, wet winters, representative of a Mediterranean Climate according to the Köppen climate classification [46]. The transition period between summer and winter is short-lived as average temperatures decline swiftly during October and November. Being a small island, the local climate is influenced by the surrounding Mediterranean Sea, which has a warming effect in winter and a cooling effect during the summer.

The Maltese Islands experience plenty of sunshine, with a daily average of 8.4 sunshine hours throughout the year and ranging from a maximum daily average of 11.2 hours in July and a minimum of 5.2 hours in December [47]. The highest temperatures are usually experienced in August, with a mean maximum temperature of 32.0°C in and a mean minimum of 23.0°C, followed by July with mean maximum and minimum temperatures of 31.7°C and 22.1°C respectively. On the other hand, the coldest months tend to be January and February, with mean minimum temperatures of 10°C and 9.6°C respectively.

In terms of precipitation, the months of November, December and January usually experience the most rainfall. Indeed, these have contributed to 16.3%, 15.5% and 14.5%, respectively, of all rainfall between 1991 and 2020. The period between May and August is almost completely dry, contributing only to 5.4% of all rainfall during the same time period [48].

With regards to wind, a clear trend in terms of direction is evident. Indeed, the most prevalent direction is the Northwest, with the wind blowing from this direction for 57% of the time. Westerly wind follows, contributing to a 22% proportion of the

Chapter 2: Literature Review

total wind direction frequency. On the other hand, mean wind speeds are fairly evenly distributed throughout the calendar months, with mean wind speeds peaking in March, April and February, all at 4.9 m s^{-1} . The summer months experience calmer winds, with August, July and September reaching an average wind speed of 3.3 m s^{-1} , 3.5 m s^{-1} and 3.7 m s^{-1} respectively [48].

Table 4: Statistics of some meteorological parameters for reference period 1991 - 2020 [47]

Month	Jan	Feb	Mar	Apr	May	Jun	Jul	Aug	Sep	Oct	Nov	Dec
Average temperature (°C)	12.9	12.6	14.1	16.4	20	24.2	26.9	27.5	24.9	21.7	17.9	14.5
Average maximum temperature (°C)	15.7	15.7	17.4	20.1	24.3	28.8	31.7	32	28.6	25	20.8	17.1
Average minimum temperature (°C)	10	9.6	10.9	12.7	15.8	19.6	22.1	23	21.2	18.4	15	11.8
Mean duration of bright sunshine (hrs)	5.4	6.6	7.2	8.4	9.9	11.2	11.9	10.9	8.4	7	6.1	5.3
Rainfall (mm)	79.4	68.9	39.7	18.7	11	7.3	0.2	11.2	59.2	77.6	89.1	84.8
Mean wind speed (m s ⁻¹)	4.6	4.9	4.9	4.9	4.5	3.9	3.5	3.3	3.7	3.8	4.2	4.7

3 Methodology

3.1 Weather Data Quality Control

In order to determine the TMY, an hourly dataset of the main meteorological parameters is a basic requirement. The quality of this dataset directly impinges on the quality and reliability of the TMY. The dataset used in this dissertation was primarily gathered by the Malta Airport Meteorological Office, or MET Office, via its monitoring stations situated at 35.853900°, 14.480457° in the Luqa airfield 79m above mean sea level¹. The MET Office also has weather stations at other localities in Malta and Gozo. The MET Office is Malta's official source for meteorological information. Indeed, the MET Office is certified in line with ISO 9001:2008 on quality measurement systems. On the other hand, the solar radiation data was obtained from the weather station of the Institute for Sustainable Energy of the University of Malta in Marsaxlokk, Malta, because the MET office does not have a full dataset for solar radiation and the global solar radiation provided was not suitable due to extreme and unreasonable values reaching 1500 W/m² during summer.

To ensure that the mentioned data was consistent, several quality control procedures were carried out over and above those carried out by the MET Office according to their ISO certification standards. These validation procedures were carried out using Microsoft Excel version 2108.

The climatological data received from the MET Office was organised in a single table containing all the parameters and the validations were carried out by using several features of the program. Firstly, general coherence checks, i.e. plausibility tests, were carried out to check that the values taken by parameters make physical sense and are in line with the respective unit of measurement. The general monthly statistics were also produced in order to detect anomalies, missing records or incomplete data. Specific validations were carried out for solar radiation to ensure

¹ Location provided by MET Office via email correspondence.

Chapter 3: Methodology

that the measurements were null between astronomical dusk and dawn, and that global solar radiation was always greater or equal to the diffuse horizontal radiation. Then, range tests were carried out to make sure that the values taken for each parameter did not exceed upper and lower limits beyond what is physically acceptable.

Another set of validations, known as step tests, were carried out. These are tests on the changes between consecutive measurements for applicable parameter and are in place to ensure that the change in parameters such as temperature, relative humidity and wind speed are in line with what is generally expected. Cases of excessive difference or stagnation between two consecutive records were vetted.

The range within which the value of a parameter is deemed as acceptable, as well as the maximum difference between two consecutive measurements, are represented in Table 5 for the applicable parameters. The acceptable limits for the range tests and step tests of the respective parameters were based on different sources of research [49], [50]. A diversity of acceptable ranges and step changes were found, and this is reasonable due to differing conditions. For example, the acceptable values depend on the location of the weather monitoring stations, as different countries and regions will tend to experience different typical and extreme climatic conditions. Secondly, the meteorological instruments utilized may vary between weather stations, which can create a disparity in accuracy and uncertainty in measurement.

The rate of recovery for each parameter of the data obtained is also presented. The rate of recovery of a parameter is defined as the number of valid measurements as a percentage of the total number of measurements that can be made in the time series, as defined by the mentioned quality control. The recovery rates are presented in Table 6 in subsection 4.1.1.

3.2 TMY Methods

There exist many methods which can be used to generate a TMY from an hourly meteorological dataset if the required variables available cover a substantial timespan. This dissertation presents the output of 5 TMY methods arising from the The Sandia National Laboratories Method, the The Danish Method and the The Festa-Ratto method. The selection process of each method has been described in detail in subchapter 2.3.2 under the respective headings. The reason for using these methods was due to several reasons. First of all, during the literature review, it arose that these methods have been used repeatedly in various TMY projects in Europe as well as in other continents. Furthermore, the selection criteria in each method are fairly diverse yet incorporate the most important variables. For example, the two methods deriving from the The Sandia National Laboratories Method, i.e. TMY_{S1} and TMY_{S2} place weight on dry bulb temperature, relative humidity, wind speed and solar radiation, but prioritise the parameters of global solar radiation and direct solar radiation, to different extents as described in Table 2. On the other hand, the The Danish Method incorporates dry bulb temperature, relative humidity, wind speed, atmospheric pressure, sunlight duration and global horizontal solar radiation for its initial point scoring system and follows up by considering the residual of the daily mean temperature, daily maximum temperature and daily sum of global solar radiation. Lastly, the The Festa-Ratto methods focus on daily mean and maximum air temperature, mean relative humidity, mean wind speed and daily sum of global solar radiation for the initial selection and vary slightly in the final selection criteria, where the TMY_{FR1} method places equal weight on the mentioned variables, whereas the TMY_{FR2} method has weighting factors as per Table 3. The variables considered in each method are shown in Table 5.

Table 5: List of parameters used by each method

	Sandia Methods		Danish Method	Festa-Ratto methods	
	TMY _{S1}	TMY _{S2}	TMY _D	TMY _{FR1}	TMY _{FR2}
Global solar radiation	Yes	Yes	Yes	Yes	Yes
Direct Solar radiation	No	Yes	No	No	No
Dry bulb temperature	Yes	Yes	Yes	Yes	Yes
Wind speed	Yes	Yes	Yes	Yes	Yes
Relative Humidity	Yes	Yes	Yes	Yes	Yes
Atmospheric pressure	No	No	Yes	No	No
Sunshine hours	No	No	Yes	No	No

The primary output of the application of the above-mentioned methods is the selection of years in which the most typical calendar month occurred. Once each typical month was determined, the various months were concatenated to form the hourly dataset with all the meteorological parameters available. The interface between the last 6 hours of the last day of a month and the first 6 hours of the first day of the following months was smoothed for dry bulb temperature, dew point temperature, wind speed, wind direction and atmospheric pressure. The smoothing was obtained by applying curve-fitting methods to the data between 12 noon of the last day of the month and 12 noon of the next day. The best possible curve was chosen on the basis of the R^2 value being the highest possible. The R^2 value of a relationship ranges from zero to one. An R^2 value of one signifies that the dependent variable is entirely described by the independent variable. Hence, a high

Chapter 3: Methodology

R^2 value ensures that the equation yielded by the regression analysis describes the relationship very well. Relative humidity was calculated by applying psychrometric relationships to the estimated dry bulb and dew point temperatures. For solar radiation, no smoothing was required, as the parameter falls to zero between each interface and transitions smoothly since solar radiation drops to zero on any day of the year. For the applicable parameters, the estimated values due to smoothing account for 1.6% of the 8760 hourly measurements.

Once the data has been smoothed, the TMY has been obtained. This enables further analysis of the results. Analysis was primarily done by comparing the outputs provided by the methods between themselves. Furthermore, the obtained outputs were compared, with the average of the 2007-2019 time series average as well as the entire 2007-2019 time series. The latter analysis was carried out by comparing the percentage frequency of the occurrence of arbitrary ranges of values taken by parameters. Wind roses were also generated using the five methods, for the 2007-2019 average and also for the entire 2007-2019 time series, and the results were also compared. The results and analyses are presented in the following chapters.

3.3 Selecting the most representative TMY

The principal aim of this dissertation is to select the TMY which is most representative of the entire time series, i.e. the meteorological data gathered from 2007 to 2019. To determine this, the TMYs were compared to the time series using the cumulative distribution function at specific percentage probabilities. The variables utilized for this analysis were the hourly dry bulb temperature, hourly wind speed and the daily sum of measurements of global solar radiation. The closeness between the CDFs of the TMYs generated and the long-term CDF will be the metric which determines the most representative TMY from the five TMYs generated.

4 Results and Analyses

4.1 Results

4.1.1 Quality Control

After running the quality control procedures mentioned in the previous chapter, a data gap for wind speed was identified, and the missing values were estimated by applying a linear regression model between the fixed meteorological station and another nearby station to obtain a linear relationship. The regression analysis for this data gap considered the measurements for the entire month in question, and the regression curve yielded a R^2 value of 0.8887. The rate of recovery for each parameter of the data was obtained and is presented in Table 6. The final rate of recovery shows the percentage of measurements which were found to be within the limits of both the step tests and plausibility tests.

Table 6: Limits for range and step tests and rate of data recovery

	Upper limit	Lower limit	Step check limit	Rate of recovery from plausibility test	Rate of recovery from step test	Final rate of recovery
Dry Bulb Temperature (°C)	40.2	1.6	±4	100%	99.87%	99.87%
Relative Humidity (%)	100	0	±15	100%	98.43%	98.43%
Atmospheric Pressure (hPa)	1067.1	985.4	±8	100%	99.99%	99.99%
Global Horizontal Radiation (Wh/m ²)	1092.3	0	Not applicable	100%	Not applicable	94.81%
Diffuse Horizontal Radiation (Wh/m ²)	628.03	0	Not applicable	94.81%	Not applicable	94.81%
Wind Speed (m/s)	28.2 ²	0	±8	100%	99.95%	99.95%

² Equivalent to Force 10 on the Beaufort scale [54]

Chapter 4: Results and Analyses

4.1.2 Typical Meteorological Months

The first direct result of the application of the TMY methods yielded the year during which the most typical month in each calendar month occurred. In most cases, different months were selected by different methods for the same calendar month. However, there were some instance where the month from the same year was chosen by different methods. There was no calendar month for which all methods agreed. There were 2 months where each of the 5 methods selected the month from different years, namely April and October.

Table 7: Typical months by TMY method

	Sandia Methods		Danish Method	Festa-Ratto methods	
	TMY _{S1}	TMY _{S2}	TMY _D	TMY _{FR1}	TMY _{FR2}
January	2008	2008	2010	2015	2010
February	2019	2008	2019	2011	2011
March	2013	2013	2008	2010	2010
April	2019	2015	2010	2017	2017
May	2012	2012	2013	2007	2007
June	2013	2011	2008	2008	2008
July	2010	2010	2008	2009	2011
August	2008	2008	2012	2014	2008
September	2011	2011	2013	2007	2007
October	2009	2018	2011	2010	2008
November	2017	2017	2007	2011	2017
December	2017	2017	2012	2011	2009

4.2 Analysis

4.2.1 Descriptive Statistics

The first assessment of the results was carried out by extracting statistics from each TMY output and to compare them with the same statistics extracted from the 2007-2019 time series. This provides initial insight into the properties of the selected typical months, the variation between different methods and their closeness to the long-term climate characteristics. This is presented for monthly and daily frequency respectively.

The tables and figures shown in the next pages serve to visually observe the closeness in the behaviour of some important parameters yielded from the TMY methods to those representing the complete time series.

The first parameter presented is the monthly mean dry bulb temperature, as shown in Table 8 and Figure 10. It is visible that the mean of the TMYs is relatively close the long-term average. Furthermore, the daily mean dry bulb temperature is also shown in Figure 13. The general trend is similar throughout. However, during most days, the long-term daily mean temperature can be observed to be lower than the daily mean temperature of the TMYs. Furthermore, the long-term mean fluctuations between consecutive days are much smaller than those of the TMYs. The long-term mean temperature was found to be 19.1°C while the means of the TMYs range between 18.8°C and 19.1°C.

The next parameter presented is the mean monthly wind speed, shown in Table 10 and Figure 11. The plotted data indicated that the monthly mean of TMYs follow the general pattern of the long-term mean. There are visible instances where the TMY mean is significantly higher or lower than the long-term average, for example in the months of March, May and December. Furthermore, the annual mean wind speed of the long-term data is 7.8 m s⁻¹ while the annual mean from TMYs varies from 7.8 m s⁻¹ to 8.9 m s⁻¹. The daily mean wind speed is shown in Figure 14.

Chapter 4: Results and Analyses

It is evident that the daily mean wind speed value covering the long-term data tends to be far smaller than the daily mean of any of the TMYs throughout the entire year. The day-to-day changes are also less pronounced. In fact, the long-term daily mean wind speed peaks at 10.6m s^{-1} whereas the peak of the TMYs range from 21.3m s^{-1} to 26.5m s^{-1} . The wind mast used by the MET Office to collect measurements is situated in the Luqa Airfield, at an elevation of 10m above ground and 81m above mean sea level.

Another parameter which is displayed for comparison is the global solar radiation. Table 11 and Figure 12 show the monthly sum of global solar radiation and the while Figure 15 shows the daily sum of global solar radiation. The monthly sums of the TMYs follow the long-term average very closely. However, the daily plot gives more insight into the differences between the long-term solar radiation and the solar radiation exhibited in the TMYs. Indeed, this relative difference is not constant throughout the year and depends on the time of year. During the warmer summer months, the long-term daily sum tends to be smaller than the other daily sums, with some occasional drops dipping below the long-term average. On the other hand, during the cooler months, the long-term daily sum spends relatively equal days above and below the daily sum of the TMYs global solar radiation. Another noticeable feature is that the global solar radiation of the TMYs undergoes significant fluctuations from one day to the next, which is not the case for the long-term data due to daily peaks and troughs being averaged out.

Chapter 4: Results and Analyses

Table 8: Monthly mean dry bulb temperatures (°C) of TMY methods and long-term data

Month	TMY _{S1}	TMY _{S2}	TMY _D	TMY _{FR1}	TMY _{FR2}	2007-2019
January	13.2	13.2	13.1	12.6	13.1	12.9
February	11.6	11.7	11.7	11.7	11.7	12.5
March	14.4	14.4	13.8	13.8	14.0	13.8
April	15.4	15.1	16.5	16.2	16.1	16.3
May	19.5	19.6	19.6	19.3	19.8	19.4
June	22.6	22.8	23.5	23.5	23.5	23.6
July	26.0	26.0	26.6	26.8	26.3	26.5
August	26.7	26.7	27.8	26.3	26.8	26.8
September	24.9	24.8	24.4	24.0	23.9	24.4
October	20.0	21.3	20.0	20.4	20.6	21.0
November	17.0	17.0	16.8	17.6	17.0	17.4
December	13.3	13.3	13.8	14.3	15.2	14.0
Annual mean	18.8	18.9	19.0	18.9	19.1	19.1

Chapter 4: Results and Analyses

Table 9: Monthly maximum dry bulb temperatures (°C) of TMY methods and long-term data

Month	TMY _{S1}	TMY _{S2}	TMY _D	TMY _{FR1}	TMY _{FR2}	2007-2019
January	17.9	17.9	19.8	17.4	19.8	21.0
February	19	17	19	19	17	24.2
March	22.4	22.4	19.9	19.9	21.5	23.5
April	27.4	25.8	23	25.7	24.4	28.6
May	27.2	27.2	26.6	28	29.2	30.4
June	33.5	31.3	32.2	32.2	32.2	38.8
July	36.2	36.2	35.4	40.2	35.5	40.2
August	35.7	35.7	38.7	33.4	35.7	38.7
September	34.2	34.2	29.5	31.9	31.9	36.1
October	25.7	27	25.9	26.1	26.1	30.0
November	22	22	22.9	22.8	22	25.0
December	20	20	19.1	19.3	22.8	22.8
Grand Maximum	36.2	36.2	38.7	40.2	35.7	40.2

Chapter 4: Results and Analyses

Table 10: Monthly mean wind speed (m s^{-1}) of TMY methods and long-term data

Month	TMY _{S1}	TMY _{S2}	TMY _D	TMY _{FR1}	TMY _{FR2}	2007 - 2019
January	4.3	4.3	5.8	5.3	5.8	4.9
February	4.7	3.6	4.7	4.5	3.5	4.9
March	5.9	6.0	5.2	5.2	4.8	5.1
April	5.2	4.3	4.7	4.9	5.2	4.9
May	4.3	4.3	5.7	5.2	4.8	4.8
June	4.4	4.3	4.4	4.2	4.2	4.0
July	3.6	3.6	3.1	3.3	3.7	3.6
August	3.0	3.0	3.0	3.3	3.0	3.3
September	3.7	3.7	3.8	4.3	4.1	3.8
October	4.3	3.9	4.3	4.4	3.1	3.9
November	4.4	4.4	4.9	4.7	4.4	4.4
December	5.0	5.0	5.2	5.1	6.0	4.9
Annual Mean	4.4	4.2	4.6	4.5	4.4	4.4

Chapter 4: Results and Analyses

Table 11: Monthly sum of global solar radiation (KW h m⁻²) of TMY methods and long-term data

Month	TMY _{S1}	TMY _{S2}	TMY _D	TMY _{FR1}	TMY _{FR2}	2007-2019
January	82.80	82.80	78.23	73.73	78.23	75.09
February	102.13	96.31	102.13	91.99	96.31	91.32
March	150.46	150.46	147.09	147.09	142.85	136.81
April	176.47	196.08	178.98	190.78	185.01	168.41
May	233.54	233.54	224.54	213.62	230.62	207.57
June	237.52	230.04	233.69	233.69	233.69	217.99
July	239.93	239.93	237.78	246.07	238.29	225.66
August	221.24	221.24	211.95	218.26	221.24	200.16
September	165.67	165.67	154.66	161.82	161.82	148.01
October	121.35	117.38	119.05	112.58	116.79	110.54
November	88.54	88.54	87.34	78.08	88.54	78.91
December	82.37	82.37	76.28	75.84	73.60	69.31
Grand Total	1902.02	1904.36	1851.73	1843.56	1867.00	1729.78

Chapter 4: Results and Analyses

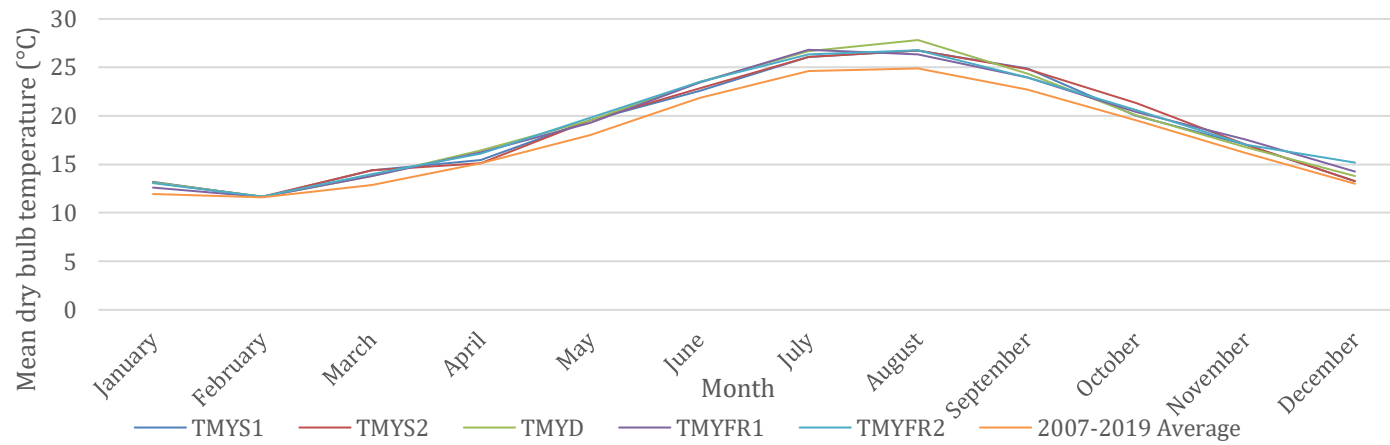


Figure 10: Monthly mean dry bulb temperatures (°C) of TMY methods and long-term data

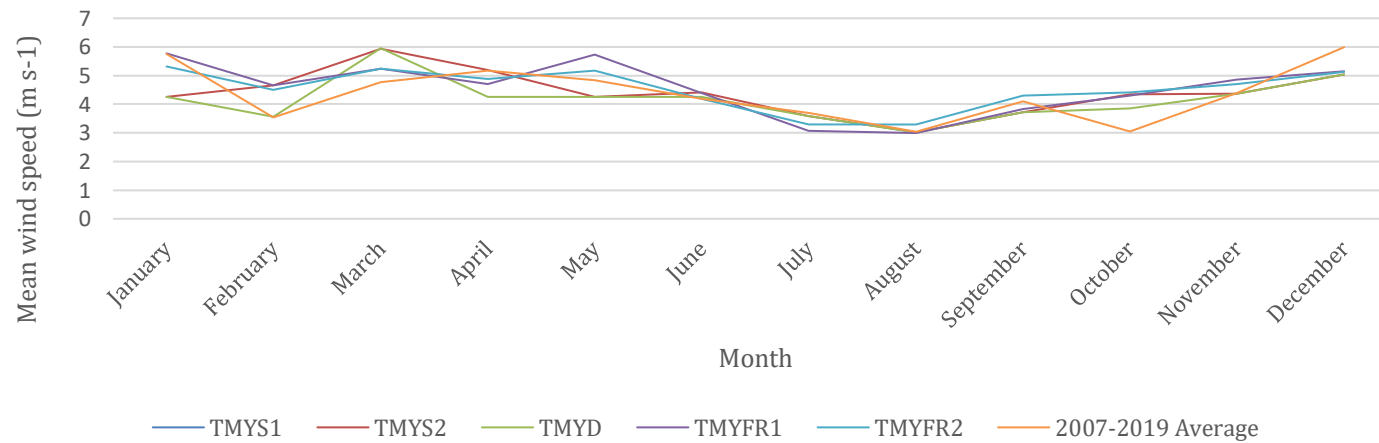


Figure 11: Monthly mean wind speed (m s⁻¹) of TMY methods and long-term data

Chapter 4: Results and Analyses

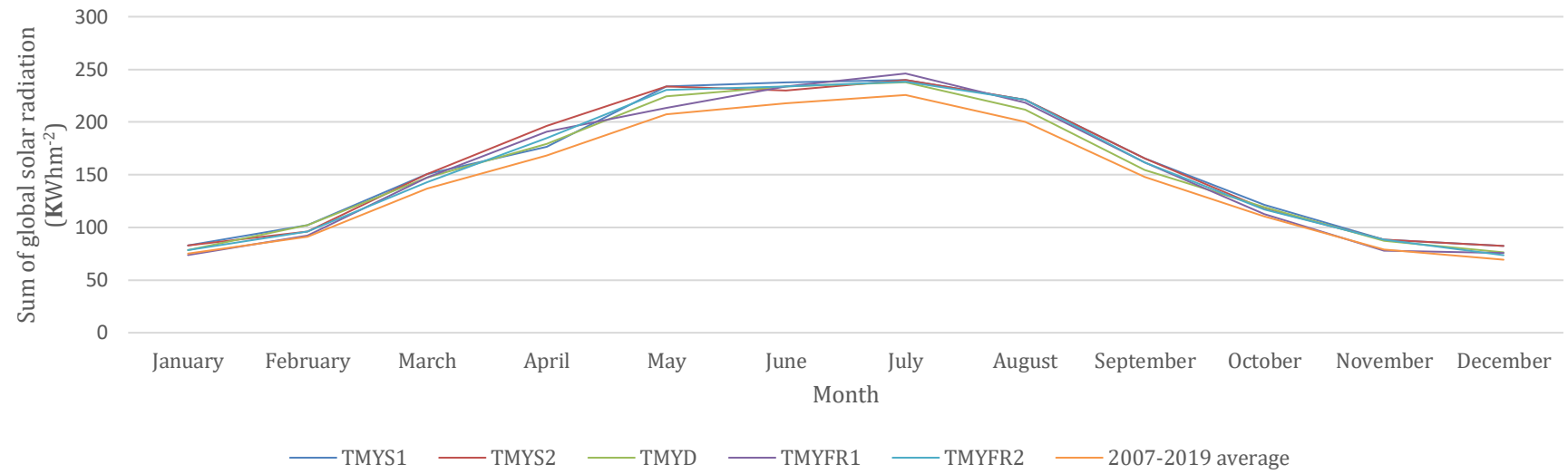


Figure 12: Monthly sum of global solar radiation (KW h m^{-2}) of TMY methods and long-term data

Chapter 4: Results and Analyses

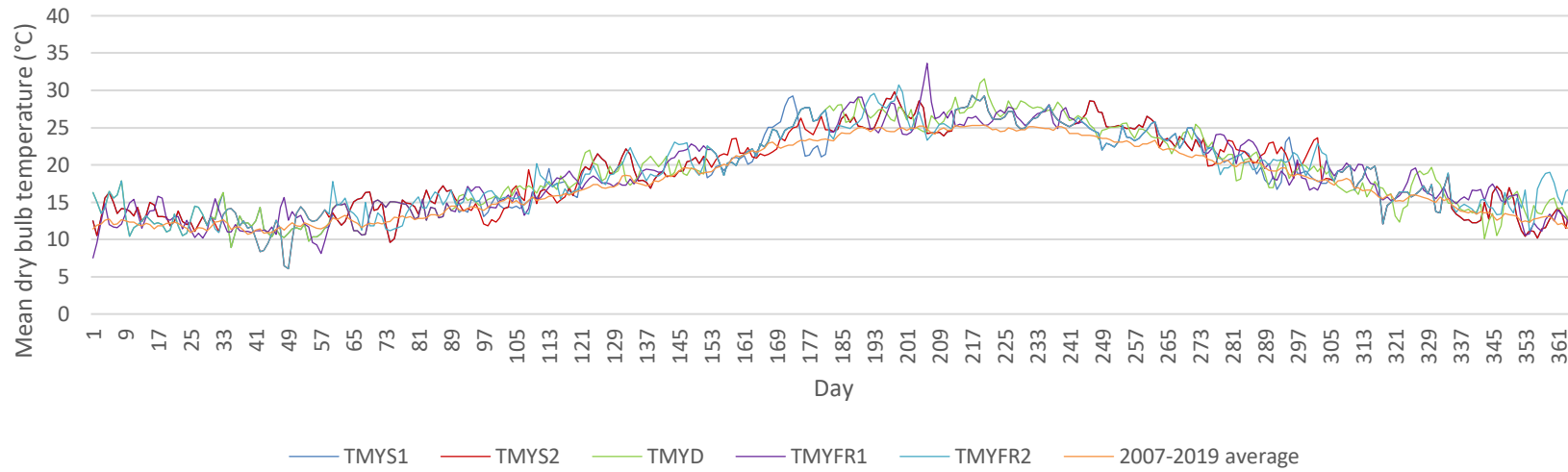


Figure 13: Daily mean dry bulb temperatures ($^{\circ}\text{C}$) of TMY methods and long-term average data

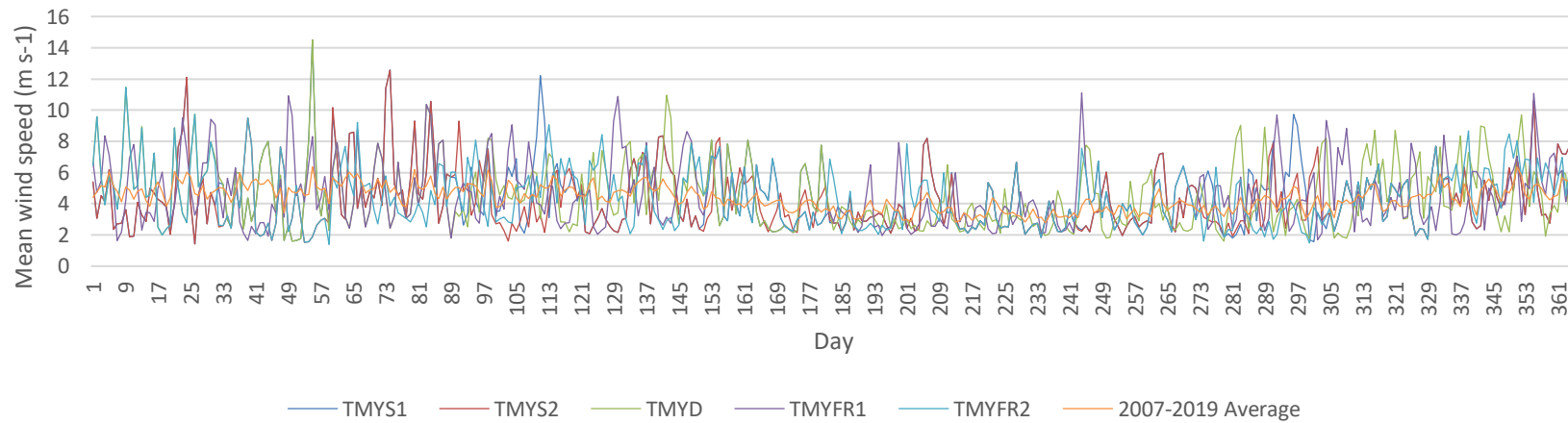


Figure 14: Daily mean wind speed (m s^{-1}) of TMY methods and long-term average data

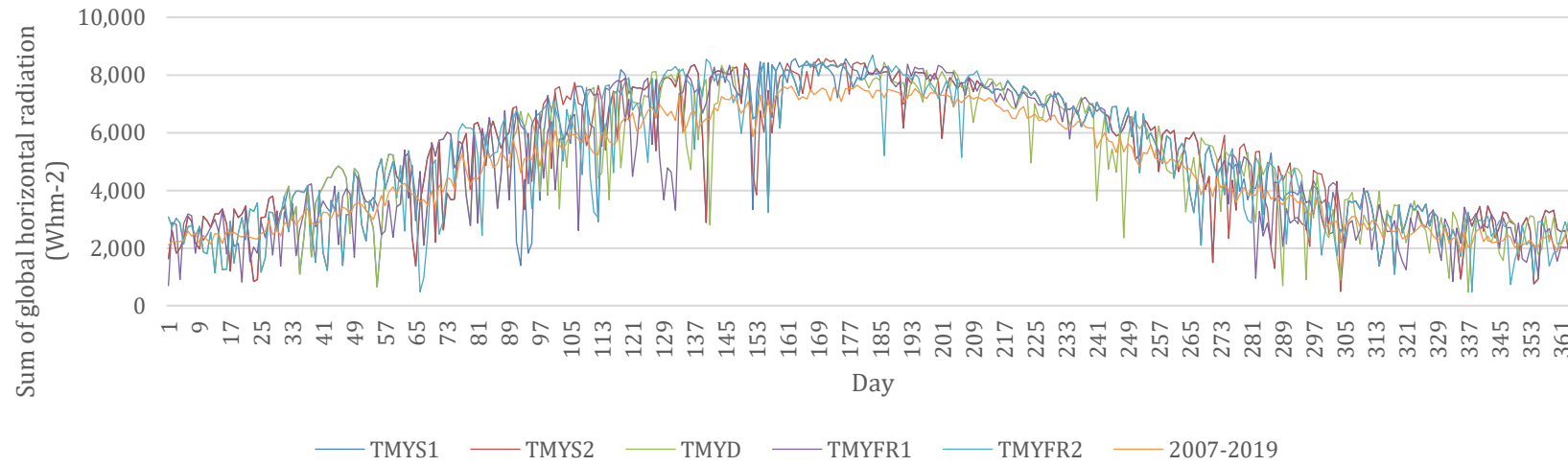


Figure 15: Daily sum of global solar radiation ($W h m^{-2}$) of TMY methods and long-term average data

4.2.2 Frequency Analysis

Further analysis on the results obtained was carried out by investigating the frequency with which the meteorological parameters were measured to be within certain arbitrarily chosen ranges. Percentage frequency analysis enables the comparison of the 13-year data to the single year TMYs without using monthly averages. For this analysis, the daily mean of dry bulb temperature, wind speed and global solar radiation were analysed by binning these values in defined ranges. The frequency with which the respective variables fell within these ranges was converted to a percentage of the total number of sample points, i.e. 365 for the TMYs and 4,745 for the long-term data.

Table 12: Dry bulb temperature percentage distribution for TMYs and long-term data

Range of Daily mean temperature (°C)	TMY _{S1}	TMY _{S2}	TMY _D	TMY _{FR1}	TMY _{FR2}	2007 - 2019
$T < 5$	0.0%	0.0%	0.0%	0.0%	0.0%	0.0%
$5 \leq T < 12$	9.6%	8.2%	9.9%	10.4%	9.1%	8.9%
$12 \leq T < 18$	39.8%	39.8%	39.3%	38.5%	37.1%	39.3%
$18 \leq T < 24$	26.1%	27.2%	25.0%	26.1%	30.2%	26.7%
$24 \leq T < 30$	24.5%	24.7%	25.3%	24.5%	23.4%	24.4%
$T \geq 30$	0.0%	0.0%	0.5%	0.5%	0.3%	0.8%

Table 13: Wind speed percentage distribution for TMYs and long-term data

Daily mean wind speed (m s ⁻¹)	TMY _{S1}	TMY _{S2}	TMY _D	TMY _{FR1}	TMY _{FR2}	2007- 2019
$0 \leq v < 3.6$	45.0%	47.5%	43.6%	42.4%	43.4%	44.8%
$3.6 \leq v < 8$	45.7%	44.9%	44.5%	46.6%	47.5%	45.5%
$8 \leq v < 12$	8.0%	6.8%	11.0%	9.9%	8.8%	8.9%
$12 \leq v < 16$	1.2%	0.8%	0.8%	0.9%	0.4%	0.7%
$v \geq 16$	0.2%	0.0%	0.1%	0.2%	0.0%	0.1%

Table 14: Global solar radiation percentage distribution for TMYs and long-term data

Daily sum of global solar radiation (W h m ⁻²)	TMY _{S1}	TMY _{S2}	TMY _D	TMY _{FR1}	TMY _{FR2}	2007 - 2019
$G = 0$	0.0%	0.0%	0.0%	0.0%	0.0%	0.0%
$0 \leq G < 600$	0.0%	0.3%	0.3%	0.0%	0.5%	0.5%
$600 \leq G < 1200$	2.2%	1.6%	2.2%	1.6%	1.6%	1.8%
$1200 \leq G < 3000$	17.3%	17.5%	20.5%	24.4%	21.4%	20.0%
$3000 \leq G < 5000$	29.0%	27.1%	27.1%	23.6%	25.2%	27.5%
$5000 \leq G < 7000$	20.3%	22.5%	21.9%	21.4%	21.6%	21.2%
$7000 \leq G < 8500$	30.7%	30.4%	27.9%	29.0%	29.0%	27.7%
$G \geq 8500$	0.5%	0.5%	0.0%	0.0%	0.5%	1.2%

Chapter 4: Results and Analyses

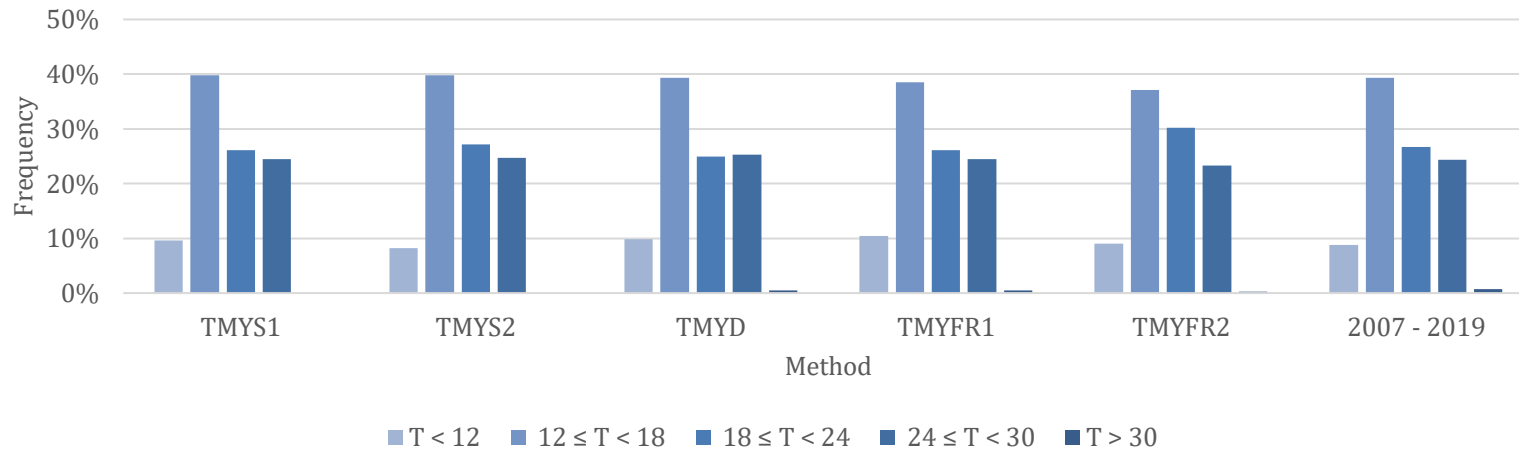


Figure 16: Daily mean dry bulb temperature (°C) histogram for TMYs and long-term data

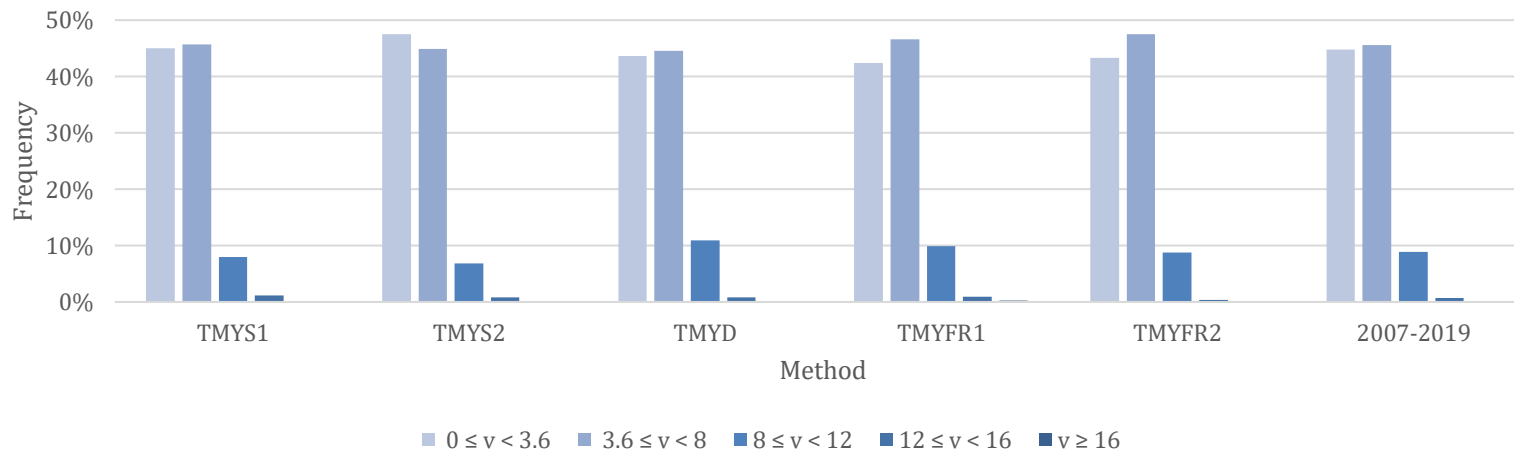


Figure 17: Daily mean wind speed (m s⁻¹) histogram for TMYs and long-term data

Chapter 4: Results and Analyses

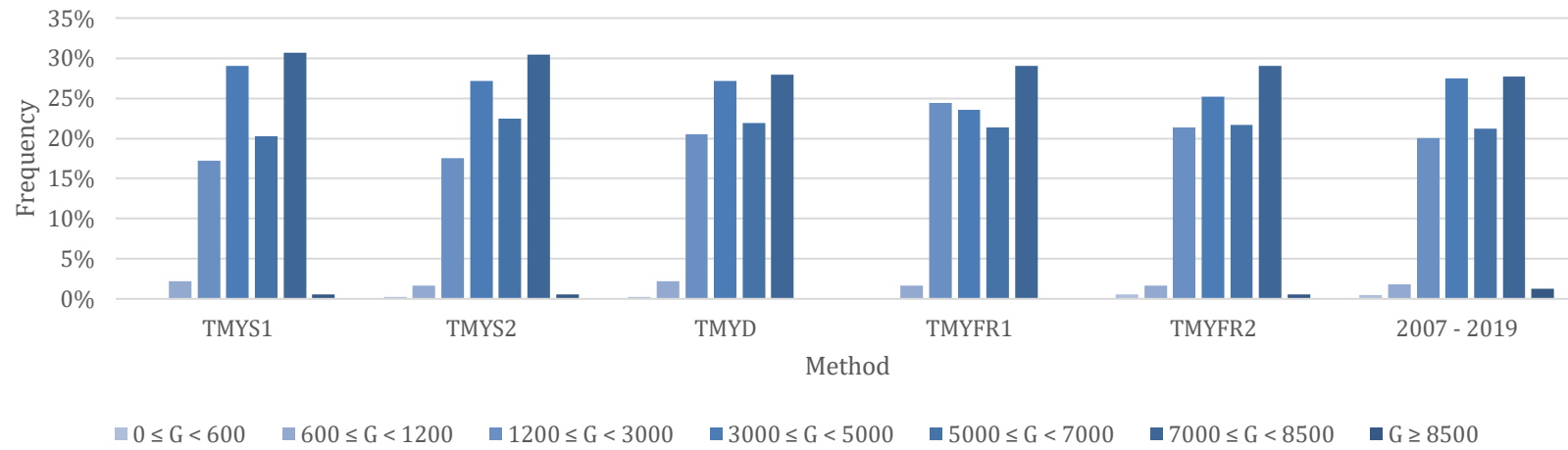


Figure 18: Daily sum of global solar radiation (W h m^{-2}) histogram for TMYs and long-term data

Chapter 4: Results and Analyses

The distribution of daily mean dry bulb temperature of each TMY as well as the entire long-term dataset are presented in Table 12 and Figure 16. The latter is presented in the form of a histogram as a graphical interpretation of the result. For all cases, the daily mean temperature falls most frequently in the range of 12°C and 18°C, where the TMYs range between 37.1% and 39.8% while for the long-term data 39.3% of days fell within this range of temperatures. The smallest and largest relative differences between the long-term data and the TMYs are 0% and 5.6% respectively. The second most common range of temperatures is that of 18°C and 24°C. Indeed, for all TMYs excluding that obtained from the Danish method, this is the second most prevalent range of daily mean temperature. The daily mean temperature of TMYs fall within this range at frequencies from 30.2% to 25.0%, while the long-term frequency was 26.7%. In this case, the smallest and largest relative differences between the long-term data and the TMYs are 1.9% and 13.1% respectively. In terms of the frequency analysis carried out, the TMYs are in close accordance with the long-term time series for the most frequent daily mean temperature range, while there is a larger relative discrepancy for the other temperature ranges.

The daily mean wind speed frequency distributions are presented in Table 13 and Figure 17. The most common daily mean wind speeds were within the range of 3.8m s⁻¹ and 8.0m s⁻¹. For the long-term data, 45.5% of days had a mean wind speed within this range, while for the TMYs, the frequency ranged between 44.5% and 47.5%. The smallest and largest relative differences were found to be 0.2% and 6.1%. The next most common range was between 0m s⁻¹ and 3.6m s⁻¹, for which the long-term data had a frequency of 44.8% while TMYs had frequencies between 42.4% and 47.5%. For this range, the smallest and largest relative differences were found to be 0.6% and 6.0%. The frequencies show that for the most frequent ranges, the TMYs have a small relative difference compared to the long-term data. Outside of the most common wind speed range, the daily mean wind speed frequencies are significantly dispersed.

For the daily sum of measurements of global solar radiation, the frequency distribution is shown in Table 14 and Figure 18. For the long-term series, the most common ranges were between 7000 and 8500 followed by the range of

Chapter 4: Results and Analyses

3000 and 5000 at 25.7% and 25.5% respectively. From Figure 18 it can be seen that all TMYs except one follow the same trend in terms of order of popularity of the top three ranges, with TMY_{FR1} following a different trend.

4.2.3 Wind direction distributions – the wind roses

Another useful tool to graphically interpret wind behaviour is a wind rose. A wind rose distributes wind speed and direction measurements onto a compass split into eight sectors representing eight directions from North to Northwest. To generate these wind roses, the hourly wind measurements were imported into WRPlot View software version 8.0.2 in the appropriate format and the results were generated using the same ranges as in Table 13 of section 4.2.2. The six wind roses are shown in this section.

Chapter 4: Results and Analyses

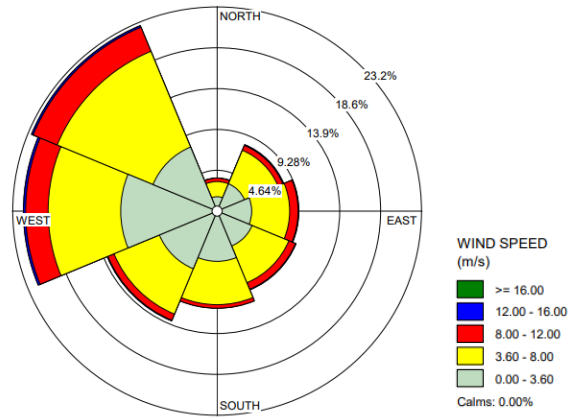


Figure 19: Wind rose for 2007-2019 hourly measurements

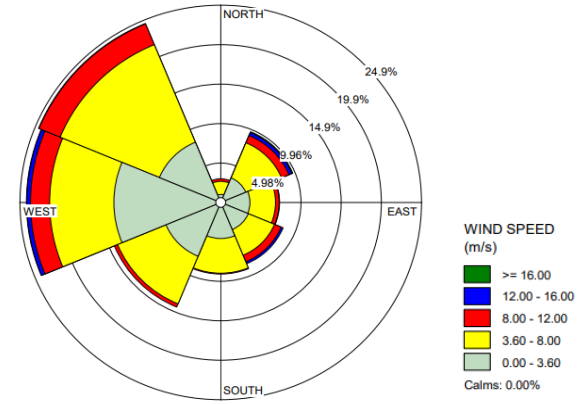


Figure 20: Wind rose for TMY₁ hourly measurements

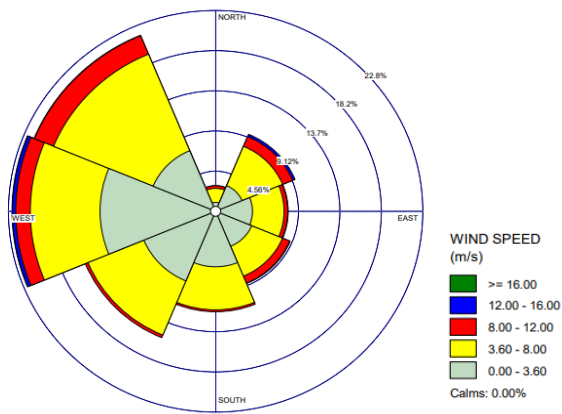


Figure 21: Wind rose for TMY₂ hourly measurements

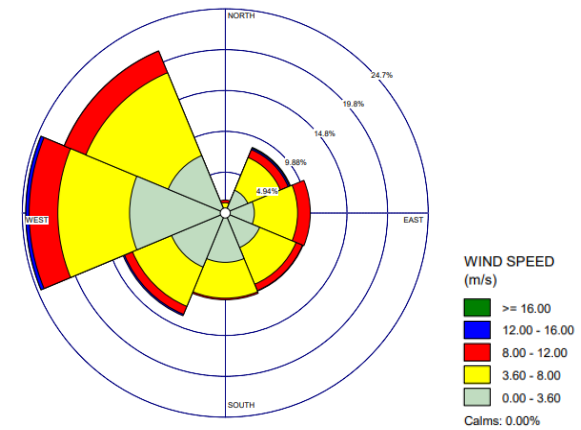


Figure 22: Wind rose for TMY_D hourly measurements

Chapter 4: Results and Analyses

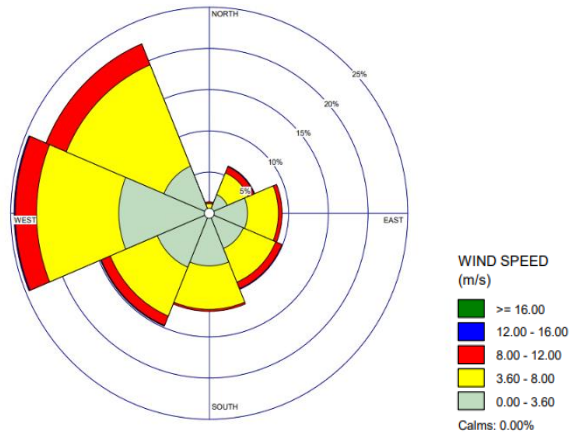


Figure 23: Wind rose for TMY_{FR2} hourly measurements

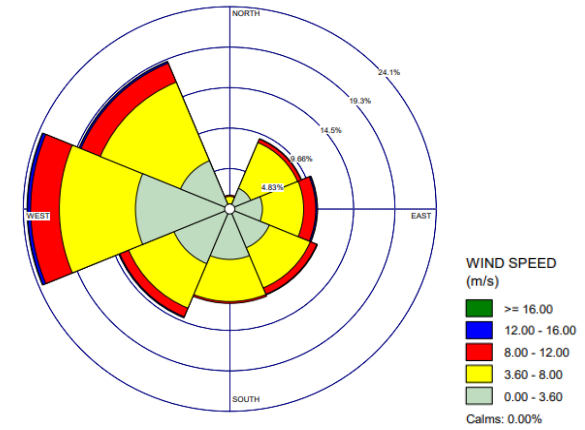


Figure 24: Wind rose for TMY_{FR1} hourly measurements

Chapter 4: Results and Analyses

4.2.4 CDF Analysis and selection of TMY

In this section, the most representative TMY from the five generated TMYs was selected. The selection criteria for the best TMY was based on the closeness of the cumulative distribution function of TMYs to that of the long-term dataset. This was determined by calculating the value taken by the CDFs of the long-term dataset and of the TMYs at certain probabilities and then finding the relative difference between each TMY and the long-term data at these probabilities. The probability points were chosen arbitrarily such that the upper and lower extremes as well as the central probabilities are included. This method was applied to the hourly dry bulb temperature, the daily sum of measurements of global solar radiation and the hourly wind speed.

The advantage of using the CDF is that the hourly data contained in the TMYs can be directly compared to the long-term hourly data. This is more favourable than comparing averages since, when taking the average, extreme values tend to cancel each other out. In principle, this analysis compares the values which have an equal probability of being recorded across the TMYs and the long-term data for each of the three parameters. The probabilities range from 0.05 to 0.95.

The first set of tables presented show the values which each parameter takes with a certain probability. The first column shows the probability being considered while the subsequent columns show the absolute value which appears with the respective probability.

Chapter 4: Results and Analyses

Table 15: Hourly dry bulb temperature (°C) values by dataset and by probability of being recorded

Probability	TMY _{S1}	TMY _{S2}	TMY _D	TMY _{FR1}	TMY _{FR2}	2007 - 2019
0.05	10.2	10.2	10.4	10.3	10.7	10.4
0.10	11.6	11.7	11.9	11.8	12.1	11.9
0.25	14.2	14.1	14.3	14.3	14.6	14.5
0.50	18.0	18.7	18.3	18.3	18.6	18.6
0.75	23.3	23.5	23.7	23.5	23.4	23.7
0.90	27.1	27.0	27.4	26.8	26.9	27.2
0.95	29.0	28.8	29.5	28.9	28.8	29.1

Table 16: Hourly wind speed (m s⁻¹) values by dataset and by probability of being recorded

Probability	TMY _{S1}	TMY _{S2}	TMY _D	TMY _{FR1}	TMY _{FR2}	2007 - 2019
0.05	1.2	1.2	1.2	1.2	1.2	1.2
0.10	1.5	1.5	1.5	1.6	1.6	1.5
0.25	2.4	2.3	2.4	2.6	2.5	2.4
0.50	3.9	3.7	4	4	4	3.9
0.75	5.9	5.7	6.3	6	6	5.9
0.90	7.9	7.5	8.3	8.3	7.9	8
0.95	9.3	8.8	9.5	9.7	8.9	9.2

Table 17: Daily sum of global solar radiation (W h m^{-2}) values by dataset and by probability of being recorded

Probability	TMY _{S1}	TMY _{S2}	TMY _D	TMY _{FR1}	TMY _{FR2}	2007 - 2019
0.05	1908.5	1873.3	1837.3	1847.3	1735.7	1727.9
0.10	2383.9	2383.9	2336.1	2113.8	2290.5	2236.5
0.25	3253.1	3225.8	3075.4	2945.3	3067.9	3109.7
0.50	5246.0	5447.4	5072.0	5076.5	5102.4	5037.5
0.75	7456.3	7447.6	7192.4	7319.0	7320.7	7281.8
0.90	8099.5	8070.3	7996.9	8085.5	8016.8	8051.9
0.95	8281.8	8281.8	8236.9	8264.5	8281.0	8274.2

The next set of tables shows the relative differences between the value of the CDF of the TMYs and that of the long-term data at each probability. In the last row, the sum of all the relative differences is calculated. A smaller sum of relative differences would indicate that the respective TMY is more representative of the long-term meteorological characteristics.

Table 18 shows that TMY_D is the best representative TMY for dry bulb temperature, with the sum of relative differences being 5.1%. This is justified since in the Danish method, two of the three parameters for which the standardized mean and standardized standard deviations are used as a selection criterion are the daily mean temperature and daily maximum temperature. It is followed by TMY_{FR1} and TMY_{FR2} with relative difference sums of 7.8% and 8.7%. The remaining TMYs have relative difference sums of 9.5% and 12.1%. The small relative differences show that overall, all the generated TMYs are highly representative of the actual long-term dry bulb temperature behaviour.

Table 18: Difference in CDF of hourly dry bulb temperature relative to long-term data by dataset and probability

Probability	TMY _{S1}	TMY _{S2}	TMY _D	TMY _{FR1}	TMY _{FR2}
0.05	1.9%	1.9%	0.0%	1.0%	2.9%
0.10	2.5%	1.7%	0.0%	0.8%	1.7%
0.25	2.1%	2.8%	1.4%	1.4%	0.7%
0.50	3.2%	0.5%	1.6%	1.6%	0.0%
0.75	1.7%	0.8%	0.0%	0.8%	1.3%
0.90	0.4%	0.7%	0.7%	1.5%	1.1%
0.95	0.3%	1.0%	1.4%	0.7%	1.0%
Sum of relative differences	12.1%	9.5%	5.1%	7.8%	8.7%

The representativeness of TMYs with respect to wind speed measurements can be determined from Table 19. Indeed the most representative TMY is TMY_{S1} whose relative difference sum is 2.3%. The next best TMY in terms of wind speed is TMY_D with a relative difference sum of 16.4%, significantly higher than that of TMY_{S1}. The remaining TMYs are also much less representative than TMY_{S1} with relative difference sums of 19.6%, 23.3% and 28.4%.

Table 19: Difference in CDF of hourly wind speed relative to long-term data by dataset and probability

Probability	TMY _{S1}	TMY _{S2}	TMY _D	TMY _{FR1}	TMY _{FR2}
0.02	0.0%	0.0%	0.0%	0.0%	0.0%
0.05	0.0%	0.0%	0.0%	6.7%	6.7%
0.10	0.0%	4.2%	0.0%	8.3%	4.2%
0.25	0.0%	5.1%	2.6%	2.6%	2.6%
0.50	0.0%	3.4%	6.8%	1.7%	1.7%
0.75	1.3%	6.3%	3.8%	3.8%	1.3%
0.90	1.1%	4.3%	3.3%	5.4%	3.3%
0.95	0.0%	0.0%	0.0%	0.0%	0.0%
Sum of relative differences	2.3%	23.3%	16.4%	28.4%	19.6%

Table 20 shows the closeness of the TMYs to the long-term dataset in terms of the global solar radiation. TMY_{FR2} is the most representative with a relative difference sum of 6.6%, followed by TMY_D and TMY_{FR1} at 14.9% and 19.5%. TMY_{S2} and TMY_{S1} follow with 28.9% and 29.5%.

Table 20: Difference in CDF of daily sum of global solar radiation relative to long-term data by dataset and probability

Probability	TMY _{S1}	TMY _{S2}	TMY _D	TMY _{FR1}	TMY _{FR2}
0.05	10.5%	8.4%	6.3%	6.9%	0.5%
0.10	6.6%	6.6%	4.5%	5.5%	2.4%
0.25	4.6%	3.7%	1.1%	5.3%	1.3%
0.50	4.1%	8.1%	0.7%	0.8%	1.3%
0.75	2.4%	2.3%	1.2%	0.5%	0.5%
0.90	0.6%	0.2%	0.7%	0.4%	0.4%
0.95	0.1%	0.1%	0.4%	0.1%	0.1%
Sum of relative differences	28.9%	29.5%	14.9%	19.5%	6.6%

The results presented in Table 18, Table 19 and Table 20 quantify the ability of each TMY in representing the complete meteorological picture. The most representative TMY is the one with the smallest relative difference over the three parameters analysed above. The sum was calculated in two ways. The first is calculated by taking the values directly from the tables such that they are equally weighted. This assumes that the dry bulb temperature, wind speed and global solar radiation are of equal importance when being used to simulate the energy performance of buildings. In this case, the smallest sum of relative differences is that of the TMY_{FR2}. The next best TMYs are the TMY_D and TMY_{S1}. The results are shown in the second row of Table 21. This ranking is due to the fact that TMY_{FR2} was the most representative of the global solar radiation data from all the methods whereas for the hourly dry bulb temperature and wind speed, it was the third most representative TMY to the other methods, although not the best.

In the previous paragraph, the three parameters were considered of equal importance in the calculation of energy efficiency of buildings. However, another way of interpreting the relative difference is to weight the parameters according to their importance on energy loads. One may consider the dry bulb temperature as being the parameter which impinges most on the use of energy in buildings and

Chapter 4: Results and Analyses

on the thermal comfort of the users. Furthermore, the wind speed and global solar radiation are taken to have the same weight. In this case, by applying weight of 0.4 for dry bulb temperature and 0.3 for wind speed and global solar radiation, TMY_{FR2} is once again the most representative of the five methods, followed very closely by TMY_D while TMY_{S1} is the third best method, therefore following the same rank as in the unweighted calculation. These results are presented in the third row of Table 21. Following this analysis, it can be concluded that the most representative TMY yielded from the five methods selected is that generated by the modified Fеста-Ratto Method, which was described in Section 2.3.2.3.

Table 21: Sums of relative difference of each TMY using equal weights and modified weights

	TMY _{S1}	TMY _{S2}	TMY _D	TMY _{FR1}	TMY _{FR2}
Equal weighting	14.45%	20.76%	12.13%	17.41%	11.69%
Modified weighting	14.22%	19.63%	11.43%	16.41%	11.39%

5 Conclusions and Recommendations

5.1 Conclusion

In this dissertation, a number of methodologies were implemented to extract the most meteorologically typical months from a 13-year dataset. Each methodology involves different statistical tools and applies them on meteorological parameters to different extents. For certain calendar months, some of the methodologies identified the same particular month from the 13 available as the most typical, as shown in subsection 4.1.2.

The analysis carried out on the results showed that the TMYs extracted exhibit varying degrees of representativity of the long-term data. The frequency analysis of the range of dry bulb temperature, wind speed and global solar radiation showed that the TMYs were fairly close to the long-term dataset for most of the ranges. This relative closeness varied with different parameters and methods. Hence, this analysis was only used as a general observation and not as a conclusive tool.

The metric used to determine the representativeness of each TMY was the cumulative distribution function evaluated at various probabilities. The relative difference between the CDF of the long-term data and that of the respective TMYs were calculated at different probabilities for hourly dry bulb temperature, hourly wind speed and the daily sum of measurements of global solar radiation. This enabled a comprehensive comparison with the 2007-2019 dataset without resorting to the use of averages, which is considered an advantage due to the loss of extreme values when taking the mean.

These relative differences were added by TMY and parameter, and the results were evaluated in two ways. Firstly, the sums were weighted equally, assuming that the dry bulb temperature, wind speed and global solar radiation have equal importance when simulating the energy use in buildings. The second result was obtained by assigning weights of 0.4, 0.3 and 0.3 to dry bulb temperature, wind

speed and global solar radiation respectively. In this way, one considers that the dry bulb temperature impinges more heavily on the energy performance of a building, with wind speed and solar radiation being equally important. The results, presented in subsection 4.2.4 showed that the level of representativeness varied depending on the parameter. Indeed, for hourly dry bulb temperatures, all of the TMYs were very truthful to the long-term series, with the sum of relative difference of the CDFs ranging from 5.1% to 12.1%. For global solar radiation, the TMYs were all acceptably close to the long-term measurements, although TMY_{FR2} excelled in particular. This was not the case for hourly wind speed, where the original Sandia National Laboratories method was the most representative of all the methods with a relative difference of 2.3%, compared to the next best method, TMY_D which achieved a relative difference of 16.4%.

When weighting the parameters of dry bulb temperature, wind speed and global solar radiation equally, the sum of relative difference in CDFs ranged from 11.7% to 20.76%. On the other hand, when prioritising dry bulb temperature with a weight of 0.4 and applying equal weight of 0.3 to wind speed and global solar radiation, the sum relative differences of the CDFs ranged from 11.4% to 19.6%. In both of these evaluations the most representative TMY was that generated by the modified Festa-Ratto method, which was labelled TMY_{FR2}, and which was presented in detail in subsection 2.3.2.3. Therefore, this dissertation found that this hourly data contained in typical meteorological year is that which should be implemented when carrying out building energy simulations for the Maltese Islands.

This dissertation managed to reach the research objectives which were set out in sub-chapter 1.4. Indeed, a selection of TMY methodologies found in literature were applied to the meteorological dataset covering the years from 2007 to 2019, which yielded five TMYs consisting of actual data extracted from the long-term data. This was followed by a thorough analysis of each TMY by comparing them amongst each other and with the long-term data using a number of metrics. Furthermore, by using the cumulative distribution function measured at different probabilities, the TMYs were classified in terms of their closeness to the long-term data and the TMY

which was most representative was identified and selected as the TMY to be implemented in building energy performance software for the Maltese Islands.

5.2 Further Work

The work carried out in this dissertation was limited by the timespan for which the required meteorological data was available. A longer timeseries would reinforce the representativity of the TMYs yielded by the respective methods since the typical months would be selected from amongst a larger pool of candidates. Therefore, the work undergone in this dissertation should be replicated in the future to incorporate a longer time frame. If the TMY is re-calculated in the future, it should also make use of the newer data which would be available at that point in time and perhaps discard older data. This is especially important in the longer term due to climate change and its effects on meteorological parameters measured. Considering the fact that extreme weather is occurring more frequently due to climate change, it is recommendable that the TMY is re-calculated using new data once available. Since the TMY developed in this dissertation covered the entire span of solar cycle 24 which lasted from 2008 until 2019, the TMY is to be re-calculated by no later than the end of the current cycle which is expected to end in 2030 [51], but it is preferable that the re-calculation is done earlier and a long-term dataset covering up to 2025 is a suitable trade-off.

Another limitation in this dissertation is the fact that the meteorological data, and hence the TMYs obtained, reflect the specific conditions of the location of the meteorological station. Ideally, hourly meteorological data would be available on a regional or district level. Although the Maltese Islands are quite small, the urban heat island effect is significant and has been found to contribute to a temperature difference of several degrees between the highly urbanised parts of Malta compared to the rural areas in both Malta and Gozo [52]. The urban heat island effect is further compounded by the fact that the more rural areas in the West and North West of Malta are situated at a much higher altitude than the more urbanized centre and East of Malta. Therefore, it would be interesting to understand how the

Chapter 5: Conclusions and Recommendations

TMY would vary across different parts of the Maltese Islands and how this could affect the cooling and heating demands of buildings.

6 References

- [1] J. Mitchell, "The "Greenhouse" Effect and Climate Change," *Reviews of Geophysics*, vol. 27, no. 1, pp. 115 - 139, 1989.
- [2] IPCC, "FAQ 1.3 What is the Greenhouse Effect?," IPCC Fourth Assessment Report: Climate Change 2007.
- [3] Centre for Science Education, "Layers of Earth's Atmosphere," 2015. [Online]. Available: <https://scied.ucar.edu/learning-zone/atmosphere/layers-earths-atmosphere>.
- [4] T. Ashton, *The Industrial Revolution 1760-1830*, Oxford University Press, 1997.
- [5] P. Friedlingstein and e. al., "Global Carbon Budget 2020," *Earth Systems Science Data*, vol. 12, no. 4, pp. 3269 - 3340, 2020.
- [6] H. Ritchie and M. Roser, "CO₂ and Greenhouse Gas Emissions," Our World in Data, 2017.
- [7] Global Monitoring Laboratory; Earth Systems Research Laboratory, "Trends in Atmospheric Carbon Dioxide" [Online]. Available: <https://gml.noaa.gov/ccgg/trends/global.html>.
- [8] Commonwealth Scientific and Industrial Research Organisation, "Latest Cape Grim greenhouse gas data" [Online]. Available: <https://www.csiro.au/greenhouse-gases>.
- [9] D. Gatley, S. Herrmann and H. Kretzschmar, "A Twenty-First Century Molar Mass of Dry Air," *Heating, Ventilating, Air-conditioning and Refrigeration Research*, vol. 14, no. 5, pp. 655 - 662, 2008.
- [10] IPCC, "Climate Change 2014: Synthesis Report. Contribution of Working Groups I, II and III to the Fifth Assessment Report of the," 2014.
- [11] European Environment Agency, "EEA greenhouse gases - data viewer".

- [12] J. Cook, D. Nuccitelli, S. Green, M. Richardson, B. Winkler, R. Painting, R. Way, P. Jacobs and A. Skuce, "Quantifying the consensus on anthropogenic global warming in the scientific literature," *Environmental Research Letters*, vol. 8, 2013.
- [13] J. Cook, N. Oreskes, P. Doran, W. Anderegg, B. Verheggen and E. Maibach, "Consensus on consensus: a synthesis of consensus estimates on human-caused global warming," *Environmental Research Letters*, vol. 11, 2016.
- [14] NASA, "Climate Change: How Do We Know?," [Online]. Available: <https://climate.nasa.gov/evidence/>. [Accessed September 2021].
- [15] R. Lindsey and L. Dahlmann, "Climate Change: Global Temperature," National Oceanic and Atmospheric Administration, March 2021. [Online]. Available: <https://www.climate.gov/news-features/understanding-climate/climate-change-global-temperature>. [Accessed September 2021].
- [16] A. Shepherd, E. Ivins, A. Geruo and V. Barletta, "A Reconciled Estimate of Ice-Sheets Mass Balance," *Science*, vol. 338, no. 6111, pp. 1183 - 1189, 2021.
- [17] University of Bonn, "Thawing permafrost releases greenhouse gas from depth," ScienceDaily, 2021.
- [18] NOAA National Centres for Environmental Information, "Global Ocean Temperature Anomalies," 2021.
- [19] H. RiebeEk and R. Simmon, "The Ocean's Carbon Balance," NASA, 2008.
- [20] Intergovernmental Panel on Climate Change, "<https://www.ipcc.ch/2021/08/09/ar6-wg1-20210809-pr/>," Geneva, 2021.
- [21] C. Aydinalp and M. Cresser, "The effects of Global Climate Change on Agriculture," *American-Eurasian Journal of Agriculture and Environment*, vol. 3, no. 5, pp. 672-676, 2008.
- [22] European Environment Agency, "Greenland and Antarctic ice sheets".

- [23] E. Schebele, "Silicon Statistics and Information," United States Geological Survey, January 2020. [Online]. Available: <https://pubs.usgs.gov/periodicals/mcs2020/mcs2020-silicon.pdf>.
- [24] K. Chia, D. Murtaugh and M. Burton, "Silicon's 300% surge throws another price shock at the world," October 2021. [Online]. Available: <https://www.mining.com/web/silicons-300-surge-throws-another-price-shock-at-the-world/>.
- [25] V. P. Masson-Delmotte, A. Zhai, S. L. Pirani, C. Connors, S. Péan, N. Berger, Y. Caud and L. Chen, "IPCC, 2021: Summary for Policymakers. In: Climate Change 2021: The Physical Science Basis," Cambridge University Press, 2021.
- [26] Climate Analytics, "Climate summit momentum: Paris commitments improved warming estimate to 2.4 C," 2021.
- [27] "Historical GHG Emissions," Climate Watch.
- [28] "Energy Balances," Eurostat.
- [29] D. Rosa and D. Maricic, "Solar Rotation," Zagreb Astronomical Observatory, October 2005. [Online]. Available: http://newserver.stil.bas.bg/SWS/lectur_1/solar_rotation.html.
- [30] "Solar Cycle Progression," Space Weather Prediction Centre (NOAA).
- [31] R. Wilson, "Solar irradiance variations and solar activity," *Journal of Geophysical research atmospheres*, vol. 87, no. A6, 1982.
- [32] I. Usoskin, "The Maunder Minimum (1645 - 1715) was Indeed a Grand Minimum: A Reassessment of Multiple Datasets," *Astronomy and Astrophysics*, vol. 581, no. A95, 2015.
- [33] S. Solanki, I. Usoskin, B. Kromer, M. Schuessler and J. Beer, "Unusual activity of the Sun during recent decades compared to the previous 11,000 years," *Nature*, vol. 431, pp. 1084 - 1087, 2004.
- [34] N. Scafetta, "Empirical Analysis of the Solar Contribution to Global Mean Air Surface Temperature Change," *Journal of Atmospheric and Solar-Terrestrial Physics*, vol. 71, pp. 1916 - 1923, 2009.

- [35] D. Mazza and E. Canuto, "Evidence of 11-Year Cycle from Sea Surface Temperature (SST)," *Academia Letters*, vol. 3032, 2021.
- [36] J. Hansen, M. Sato, V. Masson-Delmotte and F. Ackerman, "Assessing "Dangerous Climate Change": Required Reduction of Carbon Emissions to Protect Young People, Future Generations and Nature," *PLoS ONE*, vol. 8, no. 12, 2013.
- [37] G. Pernigotto, A. Prada, A. Gasparella and J. Hensen, "Analysis and improvement of the representativeness of EN ISO 15927-4 reference years for building energy simulation," *Journal of Building Performance Simulation*, 2013.
- [38] A. Argiriou, S. Lykoudis, S. Kontoyiannidis, C. Balaras, D. Asimakopoulos, M. Petrakis and P. Kassomenos, "Comparison of Methodologies using 20 years data for Athens, Greece," *Solar Energy*, vol. 66, no. 1, pp. 33 - 45, 1999.
- [39] J. Bilbao, A. Miguel, J. Franco and A. Ayuso, "Test Reference Year Generation and Evaluation Methods in the Continental Mediterranean Area," *Journal of Applied Meteorology*, vol. 43, pp. 390 - 400, 2003.
- [40] K. Hubbard, K. Kunkel, A. DeGaetano and K. Redmond, "Sources Of Uncertainty In The Calculation Of Design Weather Conditions In The Ashrae Handbook Of Fundamentals," ASHRAE, 2004.
- [41] A. Ebrahimpour and M. Maerefat, "A Method for Generation of Typical Meteorological Year," *Energy Conversion and Management*, vol. 51, no. 3, pp. 410 - 417, 2009.
- [42] H. Zang, Q. Xu, P. Du and K. Ichiyanagi, "A Modified Method to Generate Typical Meteorological Years from the Long-Term Weather Database," *International Journal of Photoenergy*, 2012.
- [43] W. Marion and M. Urban, "User's Manual for TMY2 - Typical Meteorological Years," National Renewable Energy Laboratory, 1995.
- [44] D. Crawley and L. Lawrey, "Rethinking the TMY: Is the 'Typical' Meteorological Year Best for Building Performance Simulation?," in *Building Simulation 2015*, Hyderabad, 2015.

- [45] D. Spiteri, *Night Sky Brightness of the Maltese Archipelago*, 2019.
- [46] Department of Information Malta, "The Maltese Islands," 2008. [Online]. Available: <https://web.archive.org/web/20090531132411/http://www.doi.gov.mt/en/islands/location.asp>. [Accessed March 2022].
- [47] Climatemps, "Sunshine & Daylight Hours in Luqa, Malta," [Online]. Available: <https://www.malta.climatemps.com/sunlight.php>. [Accessed January 2022].
- [48] C. Galdies, "The State of the Climate: A multidecadal report and assessment of Malta's climate," National Statistics Office, Malta, 2022.
- [49] P. Abbott, "Guidelines on the Quality Control of Surface Climatological Data," World Meteorological Office, 1986.
- [50] F. Vejen, C. Jacobsson, U. Fredriksson, M. Moe, L. Andersen, E. Hellsten, P. Rissanen, P. Palsdottir and P. Arason, "Quality Control of Meteorological Observations: Automatic Methods Used in Nordic Countries," Norwegian Meteorological Institute, 2002.
- [51] G. Hautaluoma, K. Fox, M. O'Leary, J. Leslie and P. Vanlommel, "Solar Cycle 25 Is Here. NASA, NOAA Scientists Explain What That Means," NASA, 2020.
- [52] C. Mercieca, "Measuring Urban Heat Islands using Sentinel 3," 2021 [Online] Available: <https://www.charlesmercieca.com/post/urban-heat-islands-sentinel3/>.
- [53] D. Chanette, J. Gurman and L. Acton, The Yohkoh mission of ISAS (Japan) and NASA (US), [Online]. Available: http://solar.physics.montana.edu/mckenzie/Images/The_Solar_Cycle_XRay_hi.jpg.
- [54] C. Galdies, "The Climate of Malta: Statistics, Trends and Analysis," National Statistics Office, Malta, 2011.
- [55] Chinese Academy of Sciences, "Scientists propose new formation mechanism for solar coronal rain".

- [56] National Oceanic and Atmospheric Administration, "Estimating Wind Speed," [Online]. Available: <https://www.weather.gov/pqr/wind>.